Supplementary Information

Electroassisted stable and selective CO_2 hydrogenation to methanol on CuZnAl catalyst beyond conventional thermal process

Qiang Yang, Hanwen Yan, Jie Li, Guoliang Zhang, Luming Wang, Gang Wang*, Chunshan Li*, Suojiang Zhang*

Supplementary Table 1. Detailed composition of CZA catalyst having different content of Cu element

Catalyst sample	Molar content of Cu /%	Molar ratio of Cu/Zn/Al
30%CZA	30	30/60/10
40%CZA	40	40/50/10
52%CZA	52	52/38/10
57%CZA	57	57/33/10
65%CZA	65	65/25/10

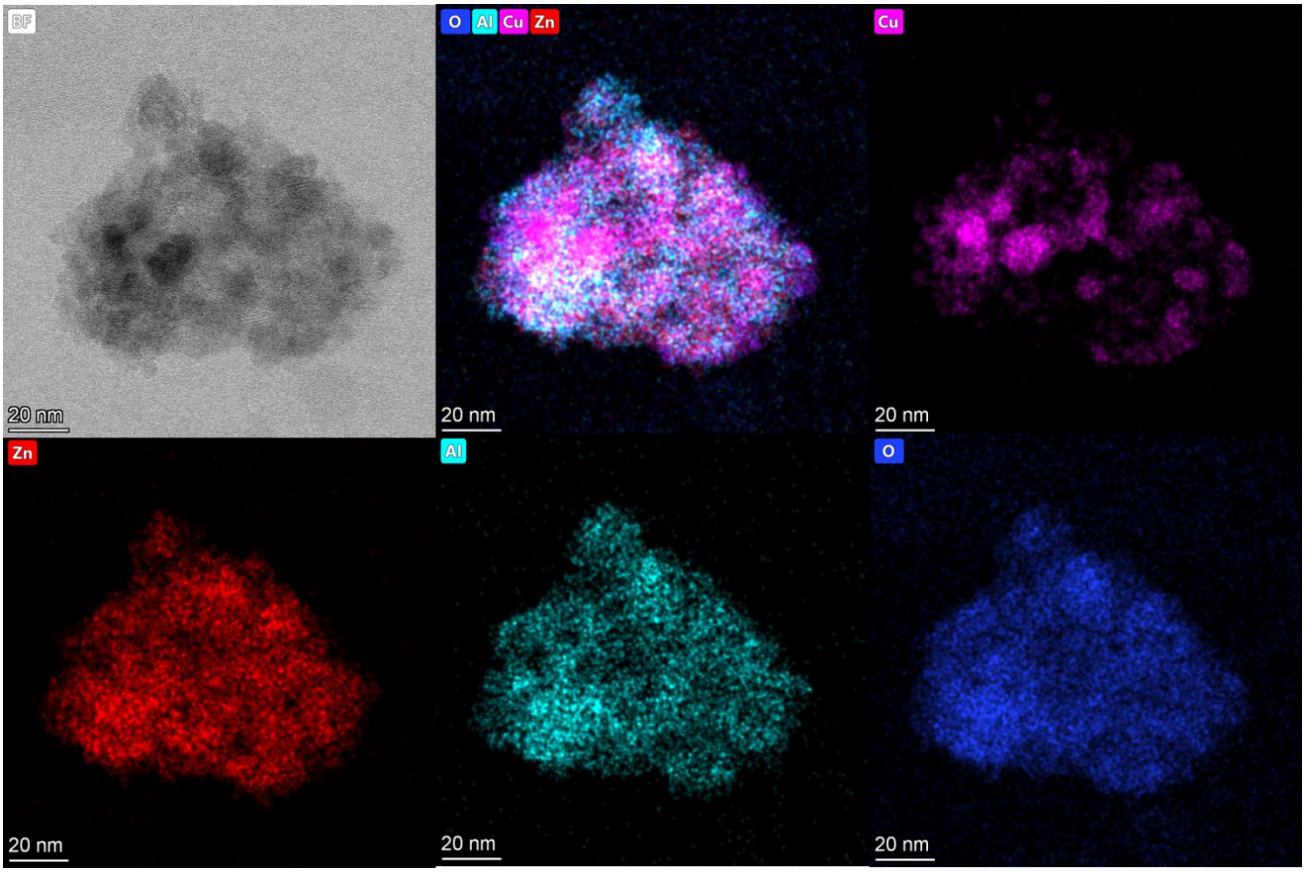

Supplementary Fig. 1 Additional representative HAADF-STEM and EDS images of 57%CZA catalyst after electroassisted treatment at the conditions of 240°C, 3 MPa, $H_2/CO_2/N_2$=72/24/4 mL·min^{-1} and 2000 mL·g_{Cat}^{-1}·h^{-1}.

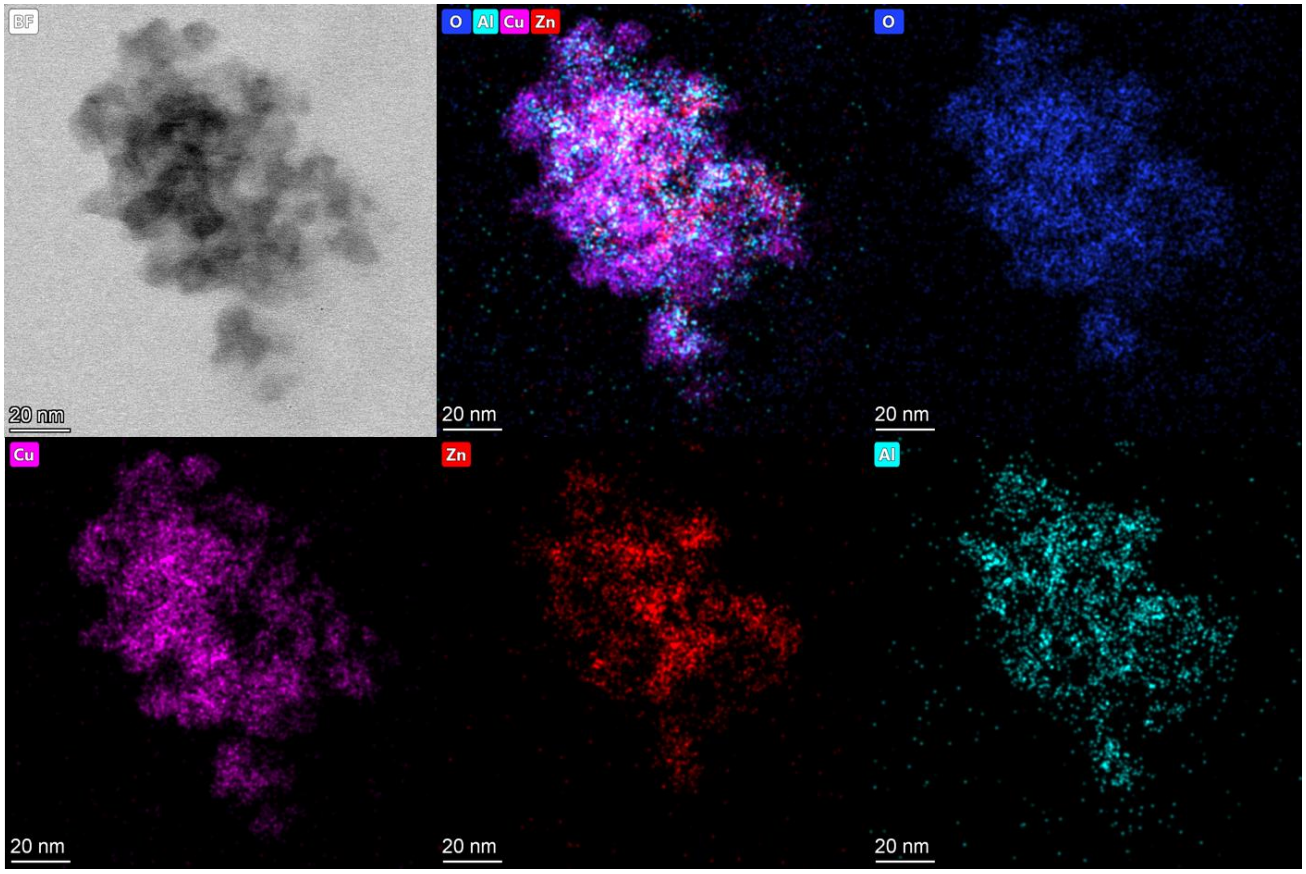

Supplementary Fig. 2 Representative HAADF-STEM and EDS images of 57%CZA catalyst after thermal treatment at the conditions of 240°C, 3 MPa, $H_2/CO_2/N_2$=72/24/4 mL·min^{-1} and 2000 mL·g_{Cat}^{-1}·h^{-1}.

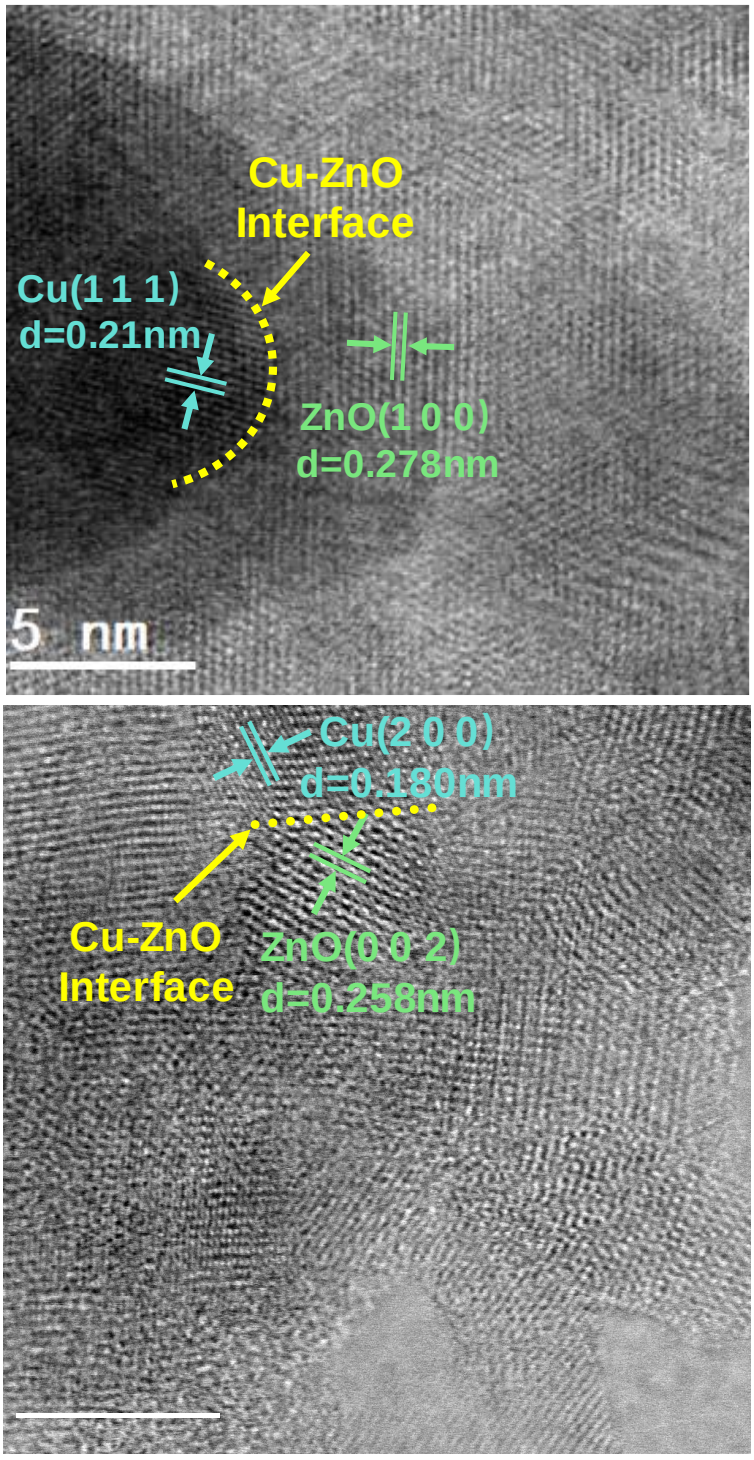

Supplementary Fig. 3 Additional representative HAADF-STEM images for the observation of Cu-ZnO interface in 57%CZA catalyst after electroassisted treatment at the conditions of 240°C, 3 MPa, $H_2/CO_2/N_2$=72/24/4 mL·min^{-1}, 2000 mL·g_{Cat}^{-1}·h^{-1} and 0.5 W.

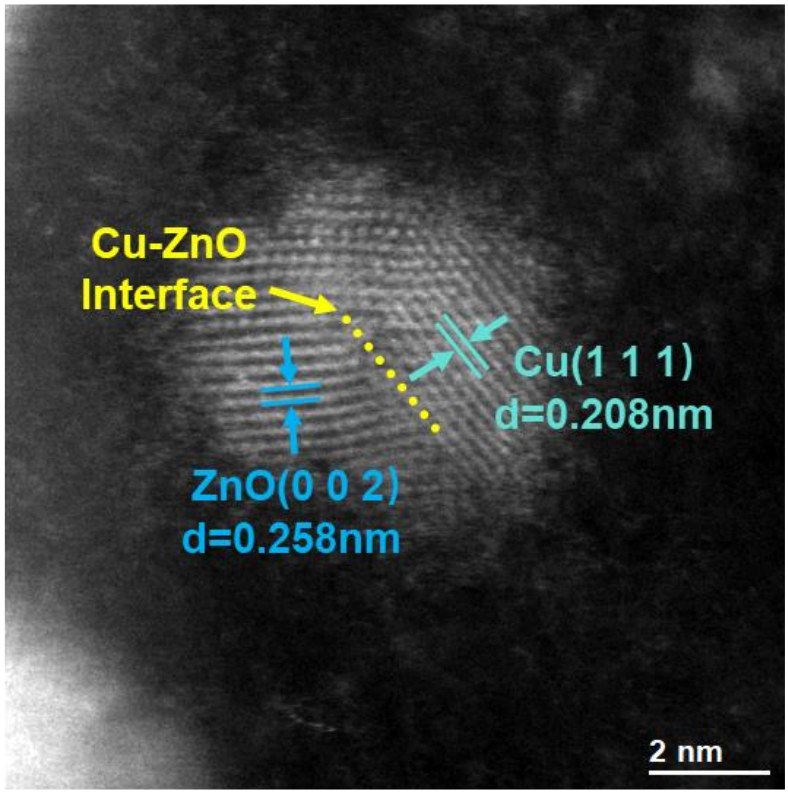

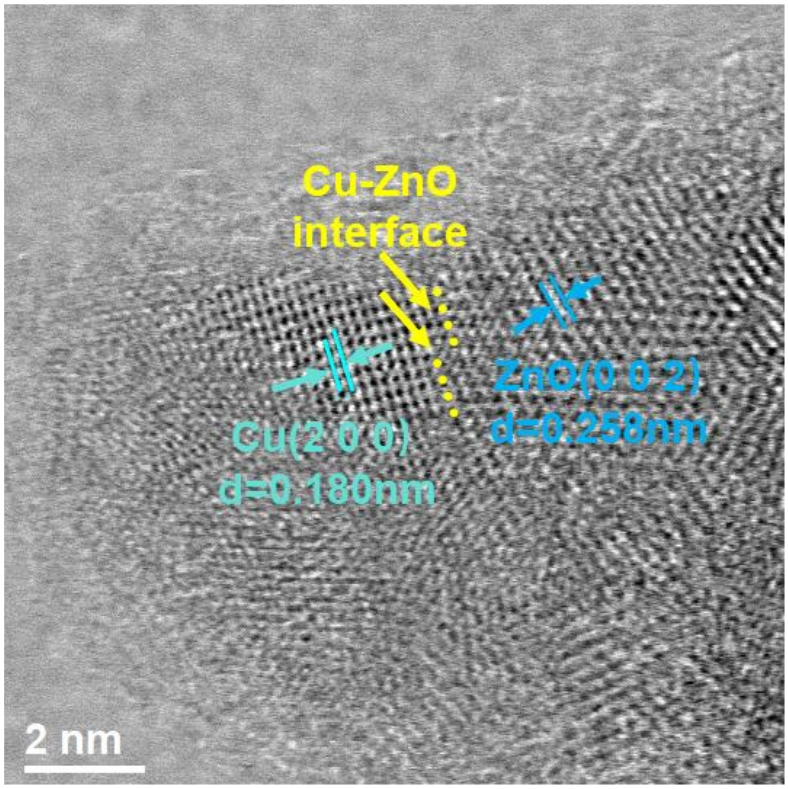

Supplementary Fig. 4 Representative HAADF-STEM images for the observation of Cu-ZnO interface in 57%CZA catalyst after thermal treatment at the conditions of 240°C, 3 MPa, $H_2/CO_2/N_2$=72/24/4 mL·min^{-1} and 2000 mL·g_{Cat}^{-1}·h^{-1}.

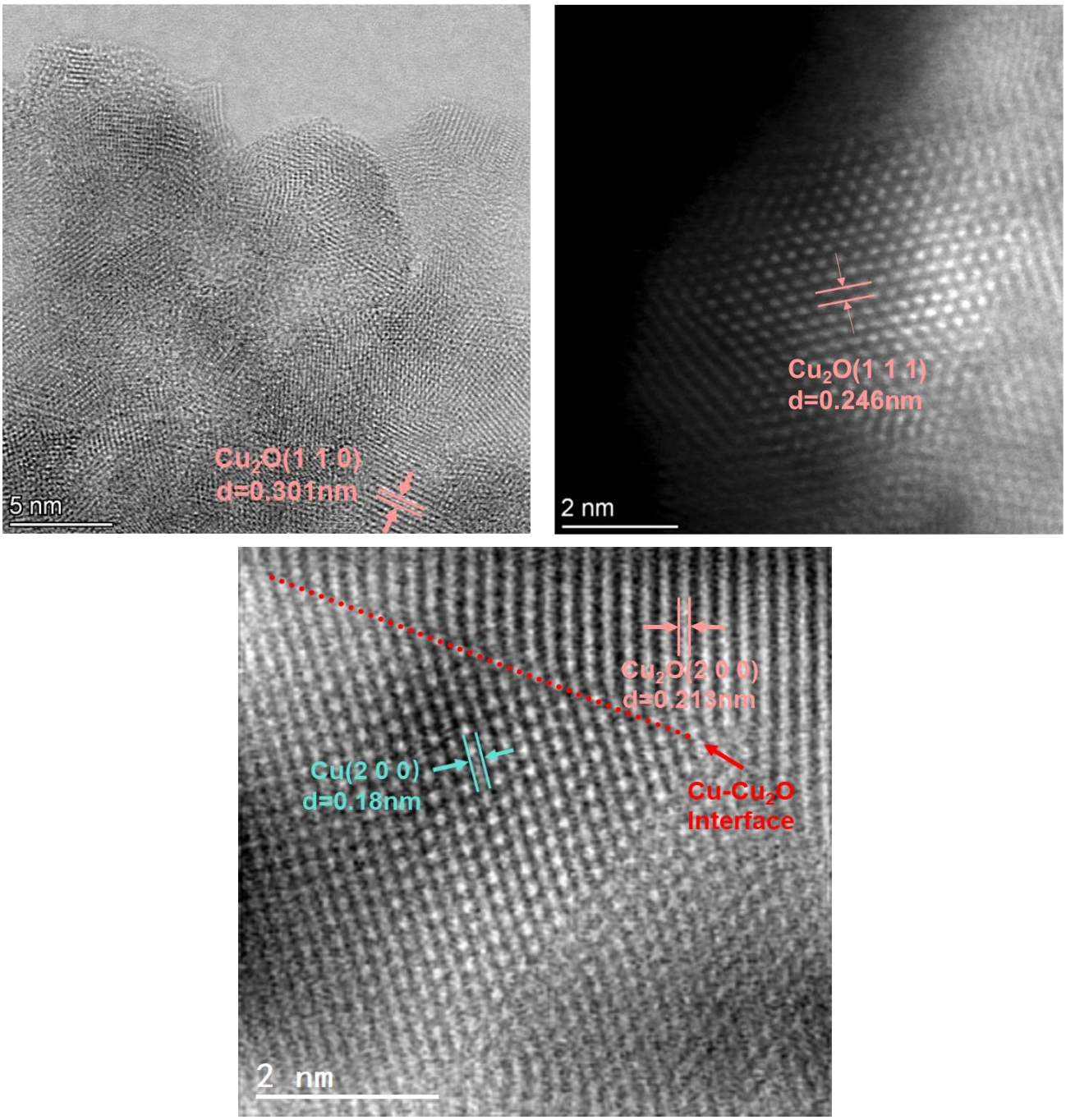

Supplementary Fig. 5 Additional representative HAADF-STEM images for the observation of Cu_2O (110) and Cu-Cu_2O interface in 57%CZA catalyst after electroassisted treatment at the conditions of 240°C, 3 MPa, $H_2/CO_2/N_2$=72/24/4 mL·min^{-1}, 2000 mL·g_{Cat}^{-1}·h^{-1} and 0.5 W.

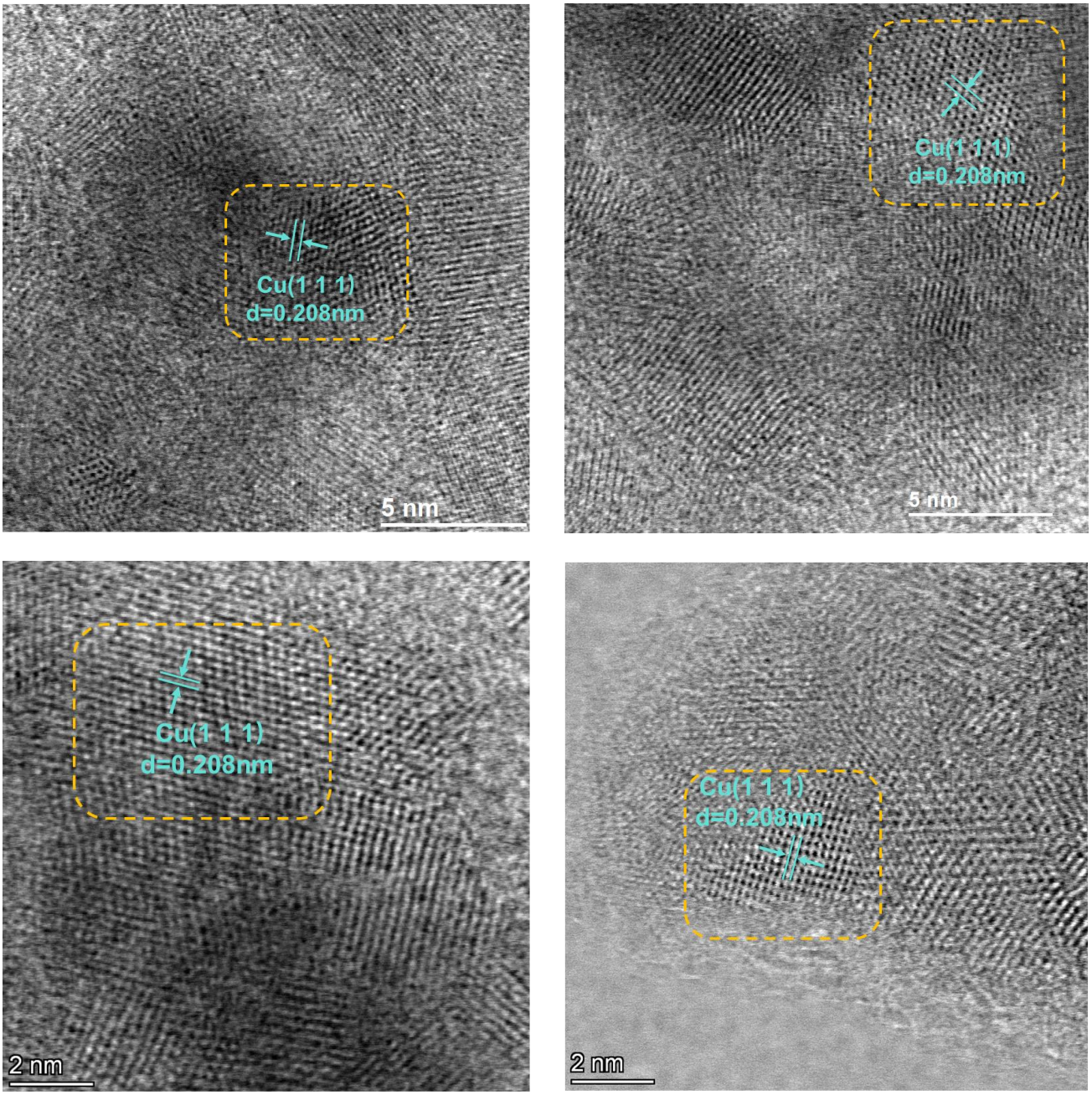

Supplementary Fig. 6 Representative HAADF-STEM images for the observation of Cu species in 57%CZA catalyst after thermal treatment at the conditions of 240°C, 3 MPa, $H_2/CO_2/N_2$=72/24/4 mL·min^{-1} and 2000 mL·g_{Cat}^{-1}·h^{-1}.

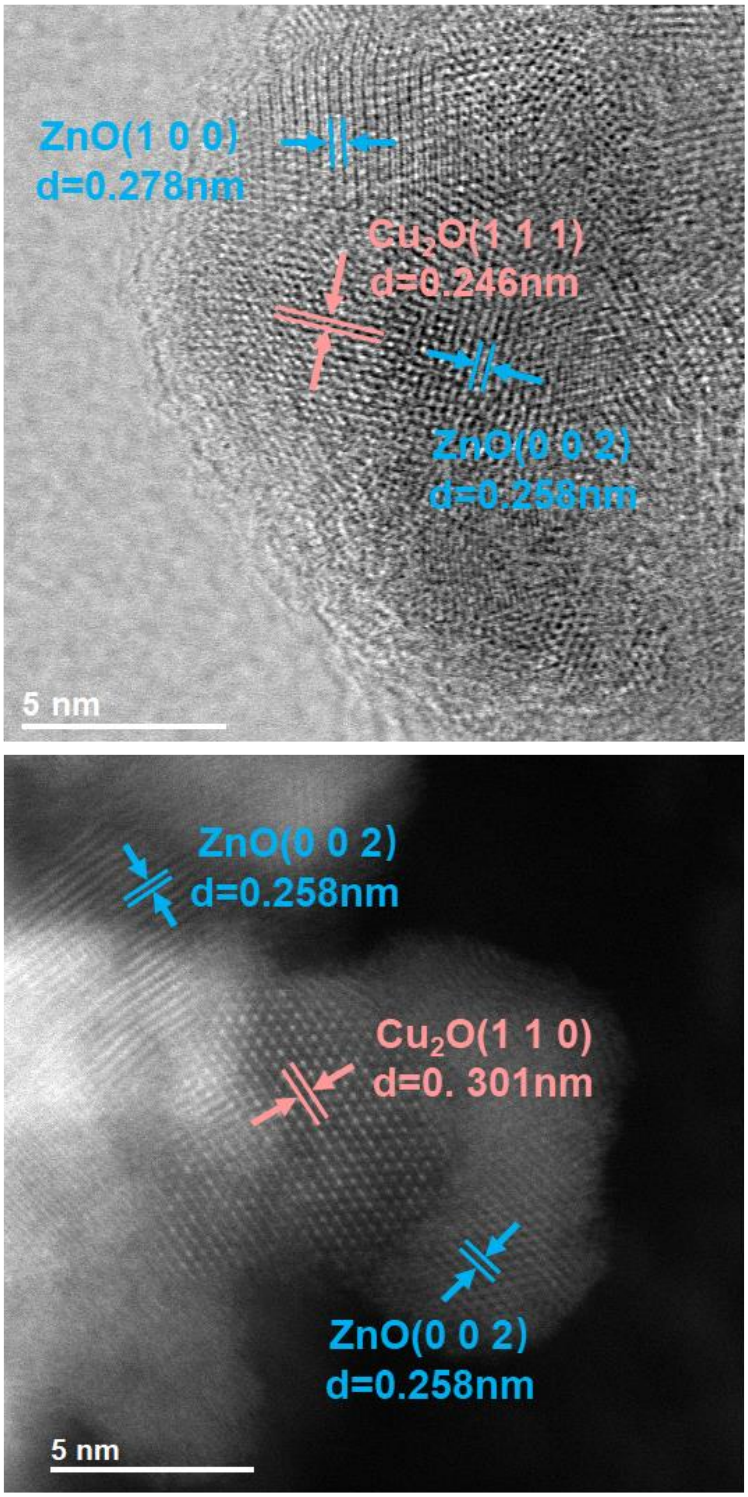

Supplementary Fig. 7 Representative HAADF-STEM images for the observation of Cu_2O (110) in 57%CZA catalyst after thermal treatment at the conditions of 240°C, 3 MPa, $H_2/CO_2/N_2$=72/24/4 mL·min^{-1} and 2000 mL·g_{Cat}^{-1}·h^{-1}.

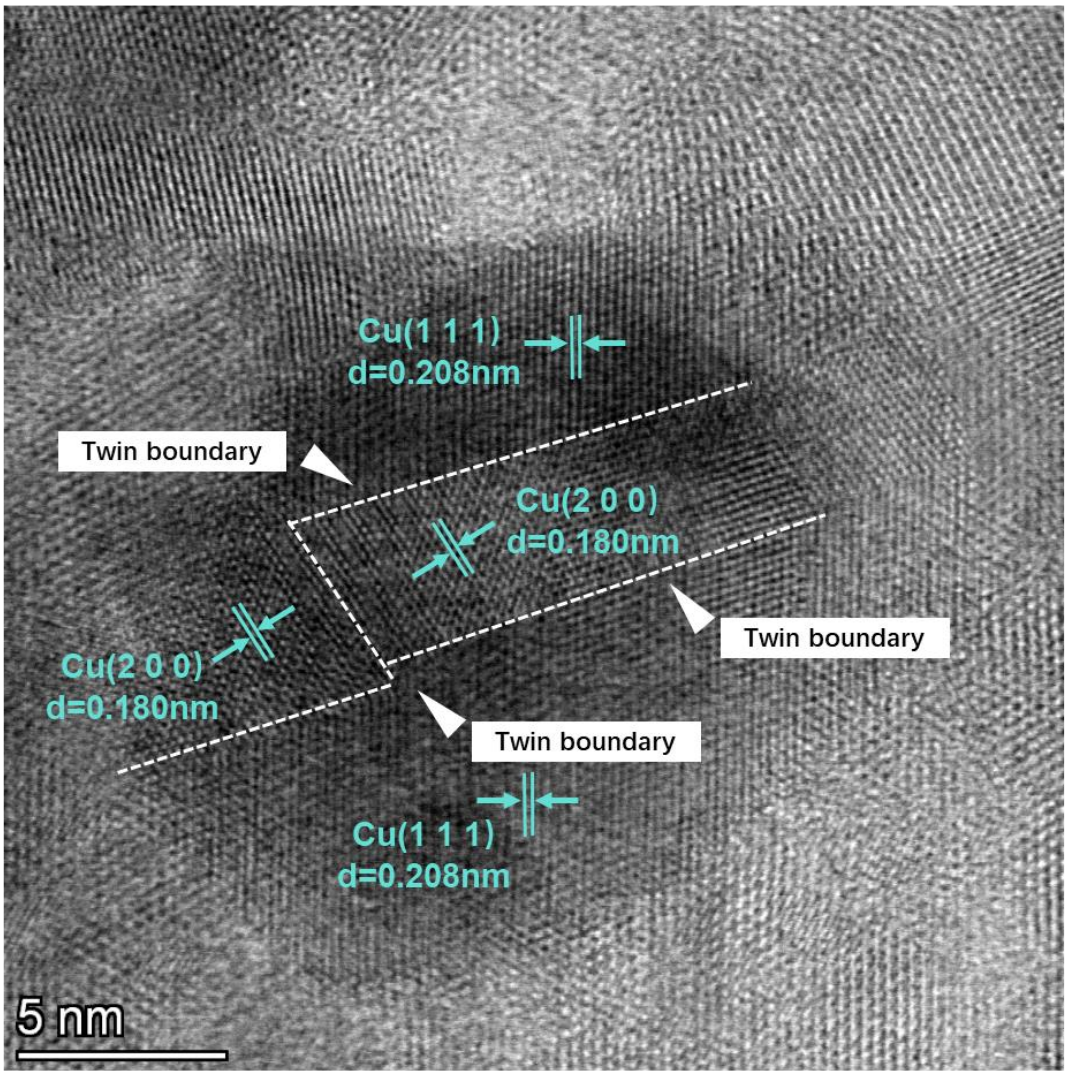

Supplementary Fig. 8 Additional representative HAADF-STEM images for the observation of twin boundary of Cu^0 species in 57%CZA catalyst after electroassisted treatment at the conditions of 240°C, 3 MPa, $H_2/CO_2/N_2$=72/24/4 mL·min^{-1}, 2000 mL·g_{Cat}^{-1}·h^{-1} and 0.5 W.

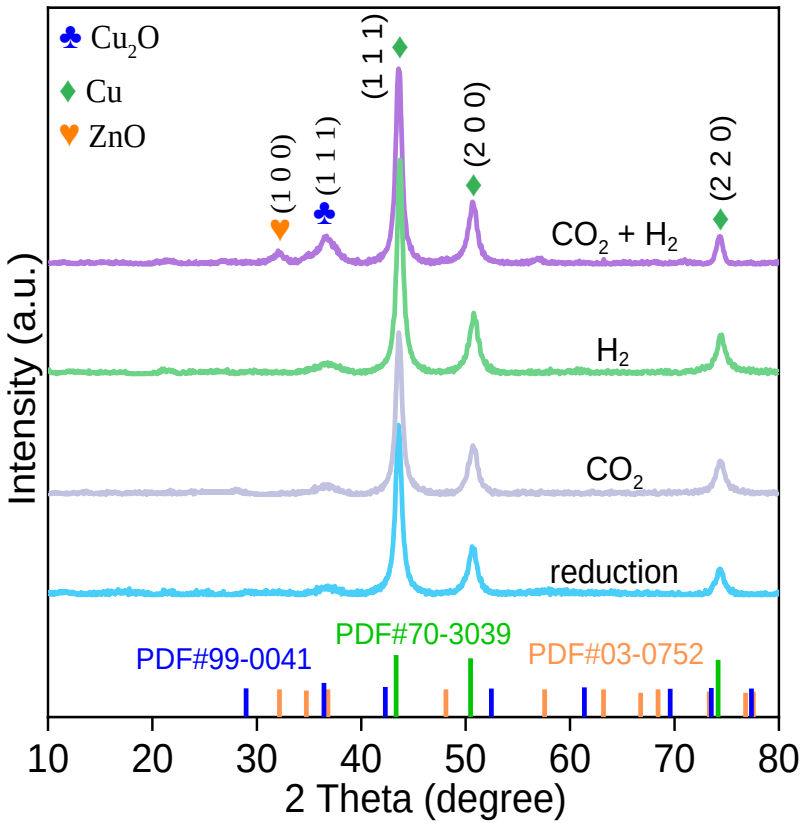

Supplementary Fig. 9 XRD patterns of 57%CZA sample recorded at the following each stage of sequentially thermal treatment using 10%H_2/N_2 (reduction pretreatment), 24%CO_2/He, 72%H_2/He, and (72%H_2 + 24%CO_2)/N_2 mixture at the conditions of 240°C, 3 MPa, and 2000 $mL \cdot g_{Cat}^{-1} \cdot h^{-1}$.

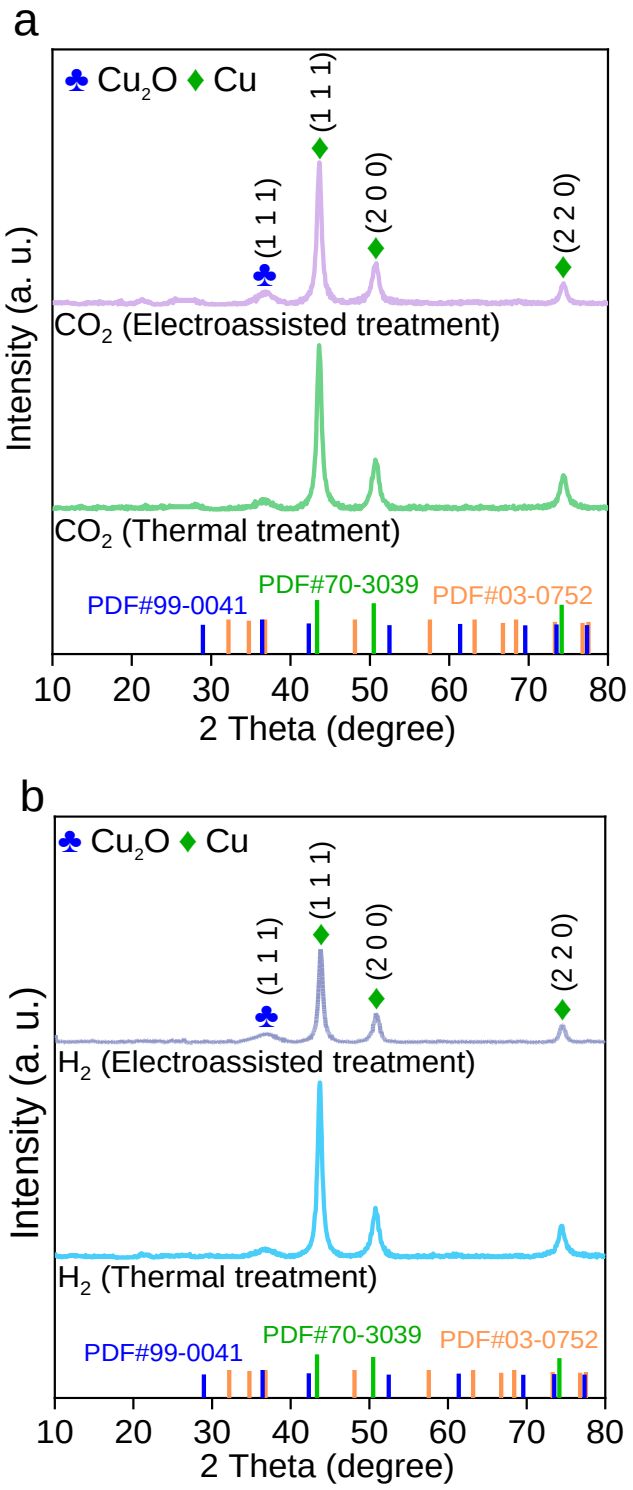

Supplementary Fig. 10 Comparison of XRD pattern of 57%CZA sample after thermal and electroassisted treatment using different gas flow of (a) CO_2 and (b) H_2 at the conditions of 240°C, 3 MPa, and 2000 $mL \cdot g_{Cat}^{-1} \cdot h^{-1}$ and 0.5 W (only for the electroassisted process).

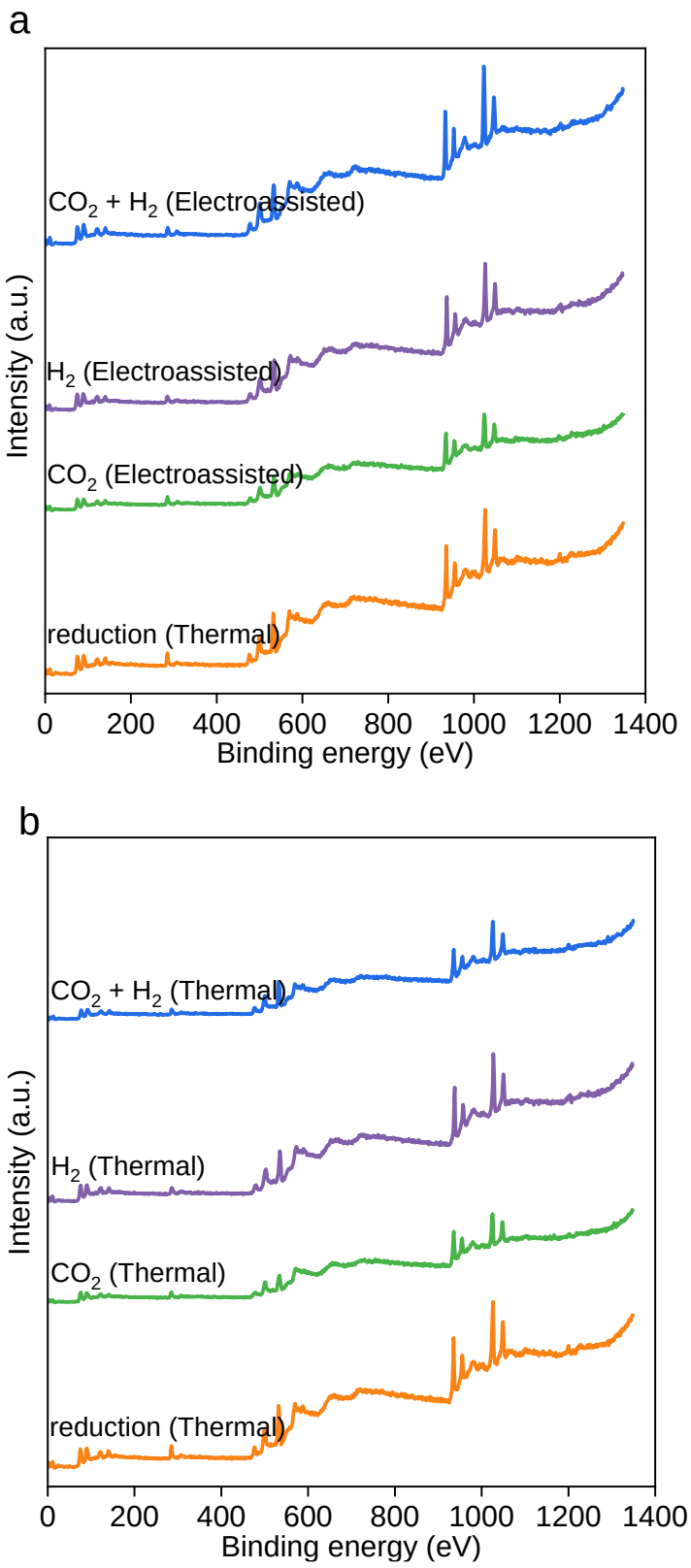

Supplementary Fig. 11 XPS survey spectra of 57%CZA catalyst sample collected at the following each stage of (a) electroassisted and (b) thermal treatment using the sequential gas flow of 10%H_2/N_2 (reduction pretreatment), 24%CO_2/He, 72%H_2/He, and (72%H_2 + 24%CO_2)/N_2 mixture at the conditions of 240ºC, 3 MPa, 2000 mL·g_{Cat}^{-1}·h^{-1} and 0.5 W (only for the electroassisted process).

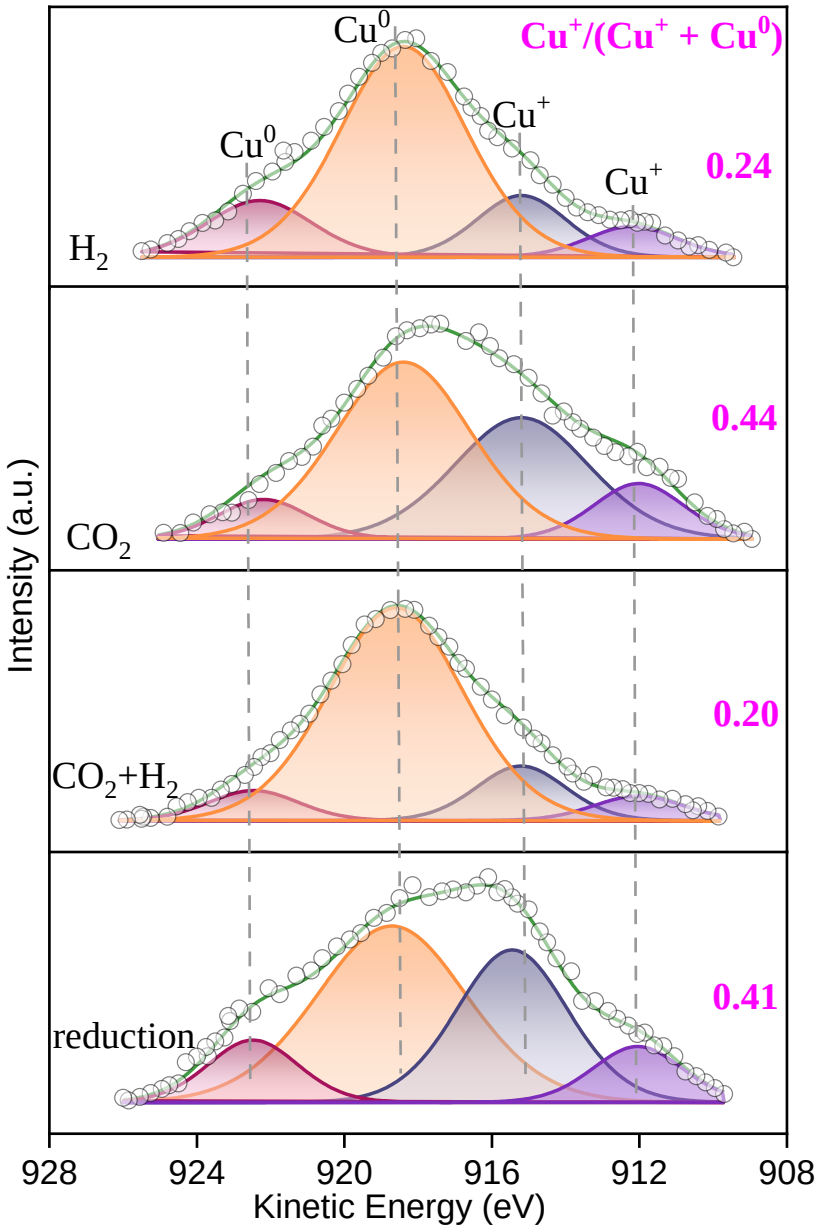

Supplementary Fig. 12 Cu LMM Auger spectra of 57%CZA catalyst sample collected at the following each stage of thermal treatment using the sequential gas flow of 10%H_2/N_2 (reduction pretreatment), 24%CO_2/He, 72%H_2/He, and (72%H_2 + 24%CO_2)/N_2 mixture at the conditions of 240°C, 3 MPa, and 2000 $mL \cdot g_{Cat}^{-1} \cdot h^{-1}$.

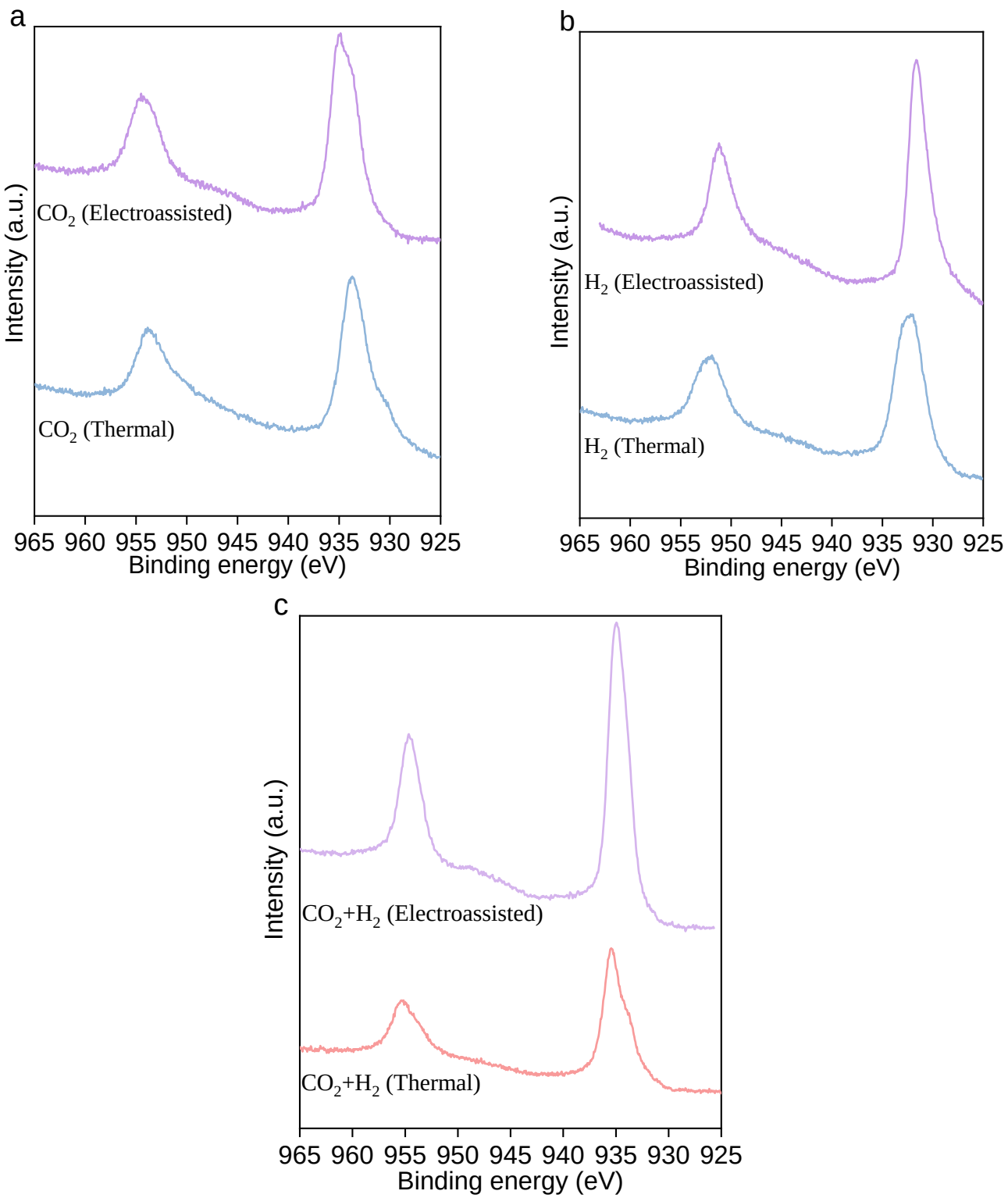

Supplementary Fig. 13 Cu 2p XPS spectra of 57%CZA catalyst sample collected at the following each stage of electroassisted and thermal treatment using the sequential gas flow of (a) 24%CO_2/N_2, (b) 72%H_2/N_2 and (c) (72%H_2 + 24%CO_2)/N_2 mixture at the conditions of 240°C, 3 MPa, 2000 $mL \cdot g_{Cat}^{-1} \cdot h^{-1}$ and 0.5 W (only for the electroassisted process) after thermal reduction pretreatment (10%H_2/N_2, 300°C).

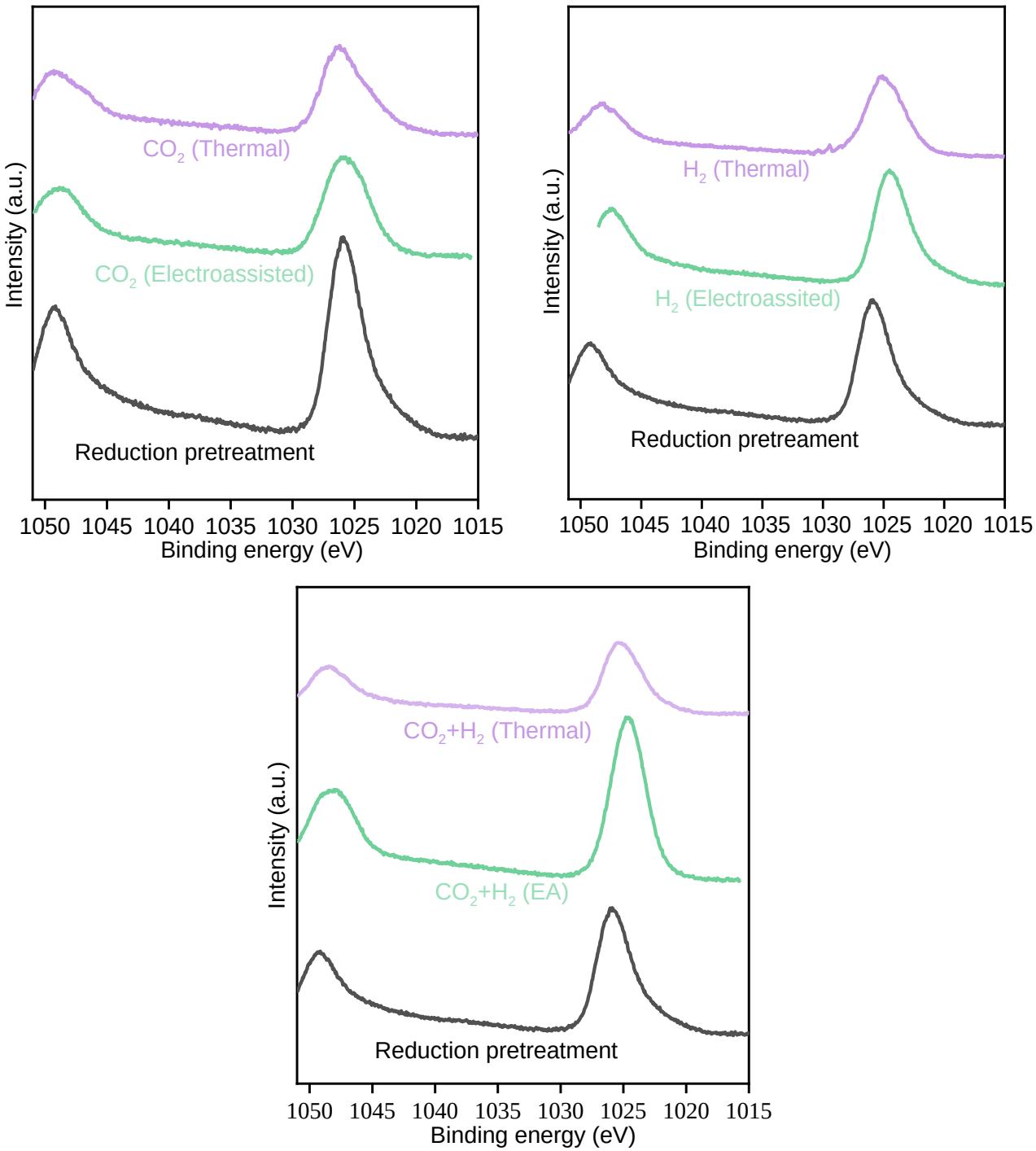

Supplementary Fig. 14 Zn 2p XPS spectra of 57%CZA catalyst sample collected at the following each stage of electroassisted and thermal treatment using the sequential gas flow of (a) 24%CO_2/N_2, (b) 72%H_2/N_2 and (c) (72%H_2 + 24%CO_2)/N_2 mixture at the conditions of 240ºC, 3 MPa, 2000 mL·g_{Cat}^{-1}·h^{-1} and 0.5 W (only for the electroassisted process) after thermal reduction pretreatment (10%H_2/N_2, 300ºC).

Supplementary Table 2 XPS analysis results of the surface Cu and Zn composition

Sample	Surface element composition (%)		Cu/(Zn+Cu)
	Cu	Zn	
57%CZA_Reduction	14.08	15.31	0.48
57%CZA_CO_2+H_2_Electroassisted	12.01	18.95	0.39
57%CZA_CO_2+H_2_Thermal	12.55	16.94	0.42

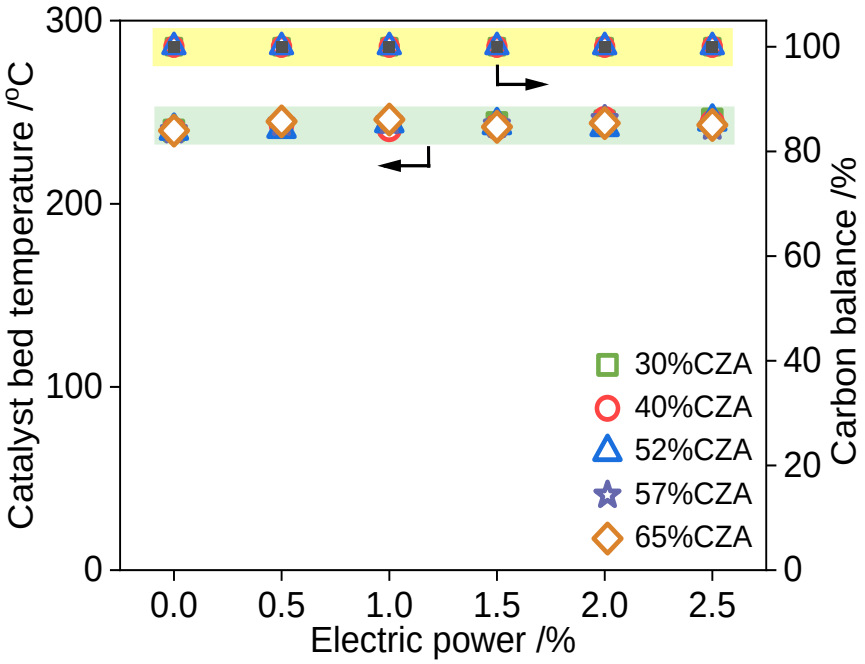

Supplementary Fig. 15 Catalyst bed temperature and carbon balance during electroassisted CO_2 hydrogenation at the conditions of 240°C, 3 MPa, and 2000 $mL \cdot g_{Cat}^{-1} \cdot h^{-1}$ and 0.5 W.

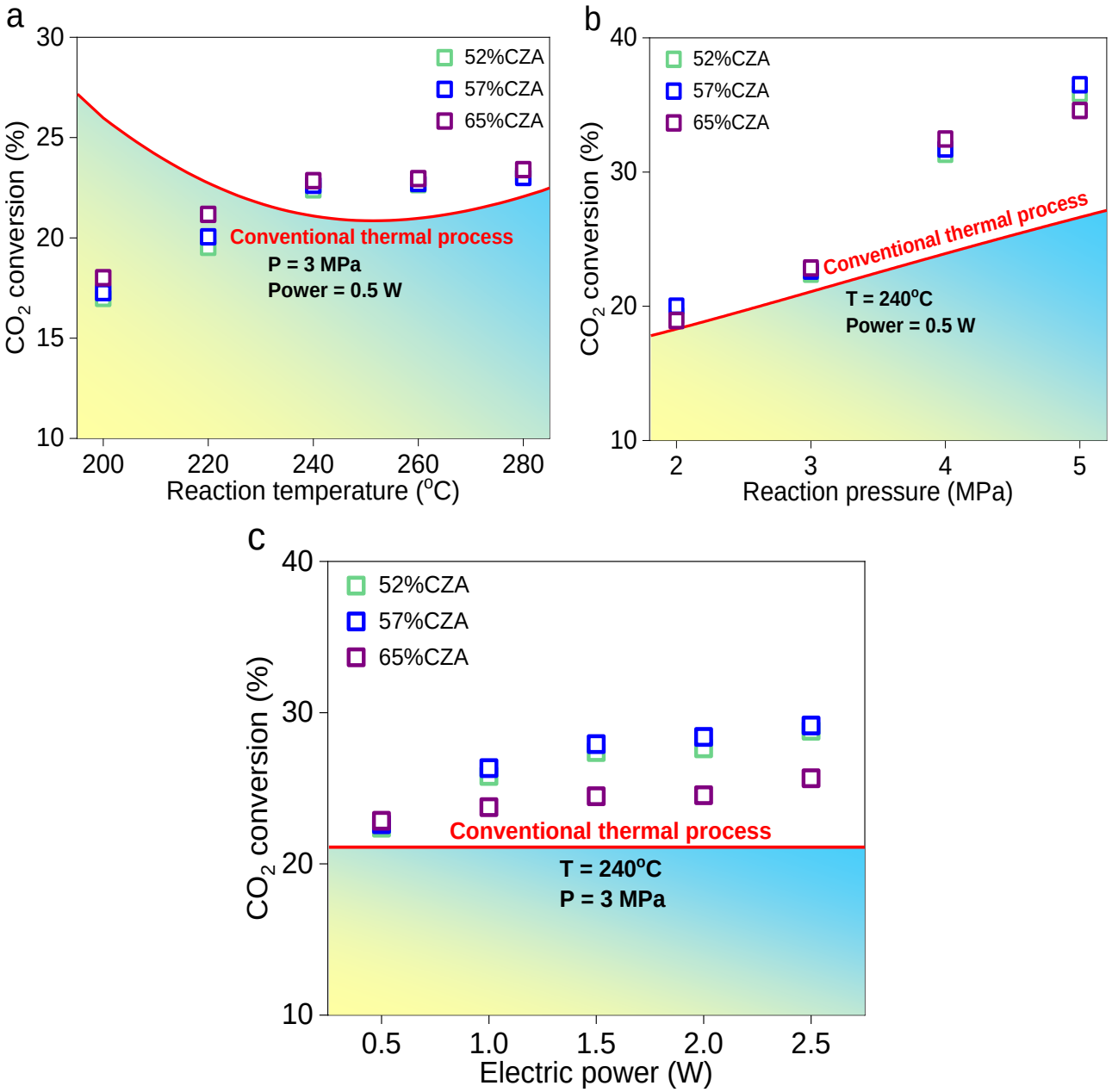

Supplementary Fig. 16 Comparison between the conventional thermal process and electroassisted catalytic results at different temperatures, pressures and electric powers under the other conditions of $H_2/CO_2/N_2$=72/24/4 mL·min^{-1} and 2000 mL·g_{Cat}^{-1}·h^{-1}.

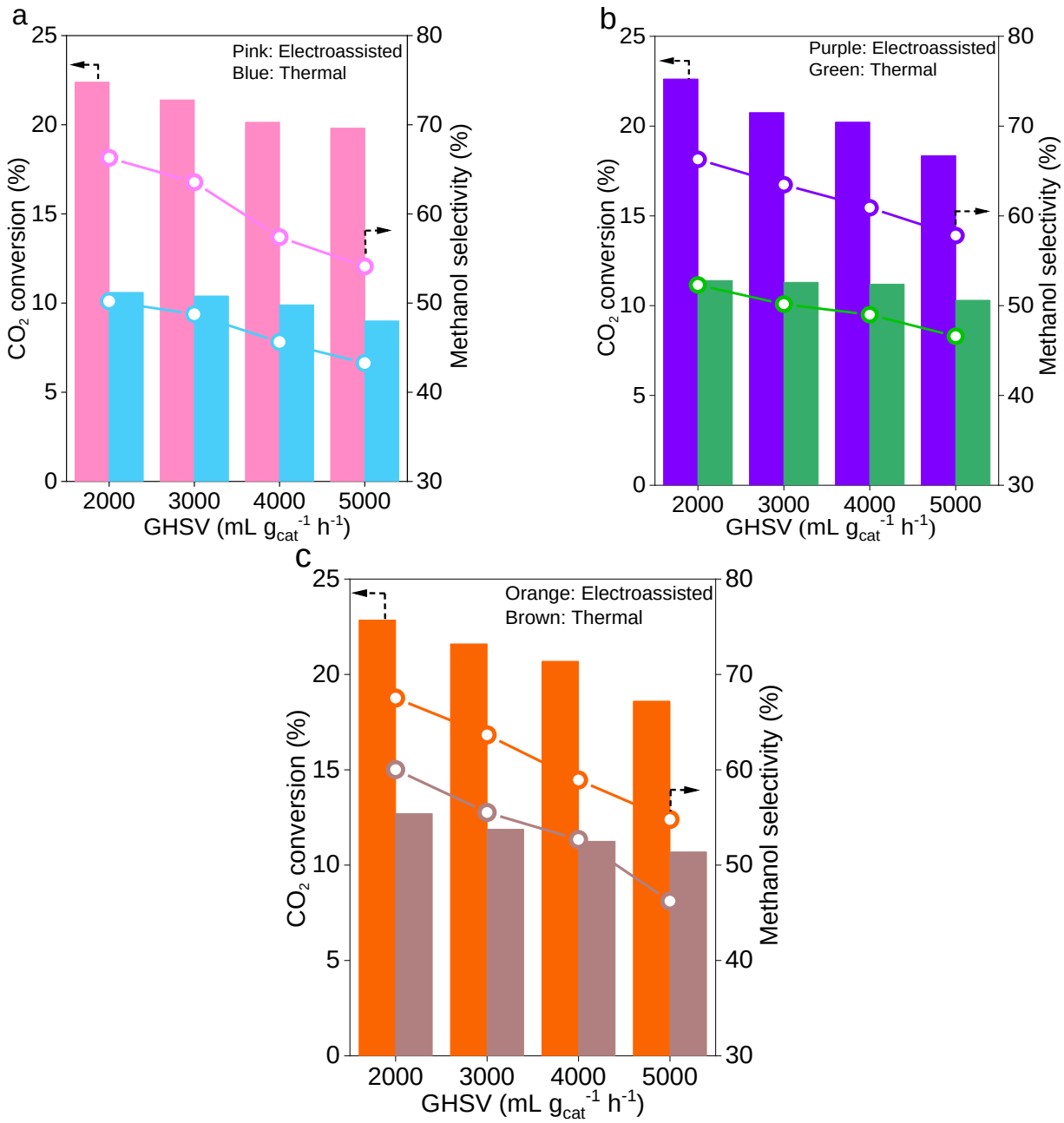

Supplementary Fig. 17 Effect of space velocity on the electroassisted catalytic CO_2 selective hydrogenation to methanol on (a) 52%CZA, (b) 57%CZA and (c) 65%CZA at 240°C, 3.0 MPa, 0.5 W, H_2/CO_2 ratio = 3 and 3 g catalyst compared those results obtained under thermal condition.

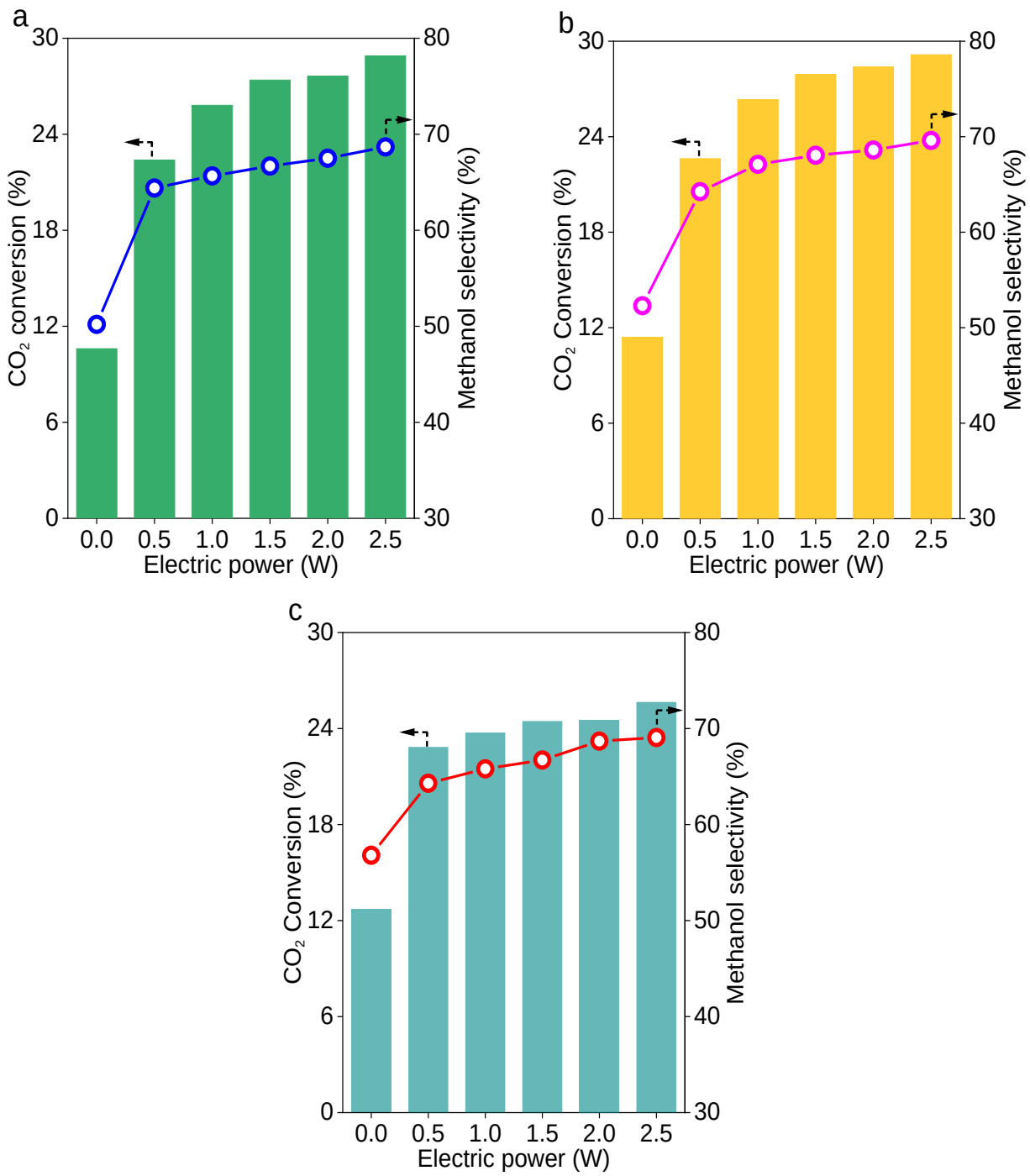

Supplementary Fig. 18 Effect of space velocity on the electroassisted catalytic CO_2 selective hydrogenation to methanol on (a) 52%CZA, (b) 57%CZA and (c) 65%CZA at 240°C, 3.0 MPa, 2000 $mL \cdot g_{Cat}^{-1} \cdot L^{-1}$ and H_2/CO_2 = 3 compared those results obtained under thermal condition.

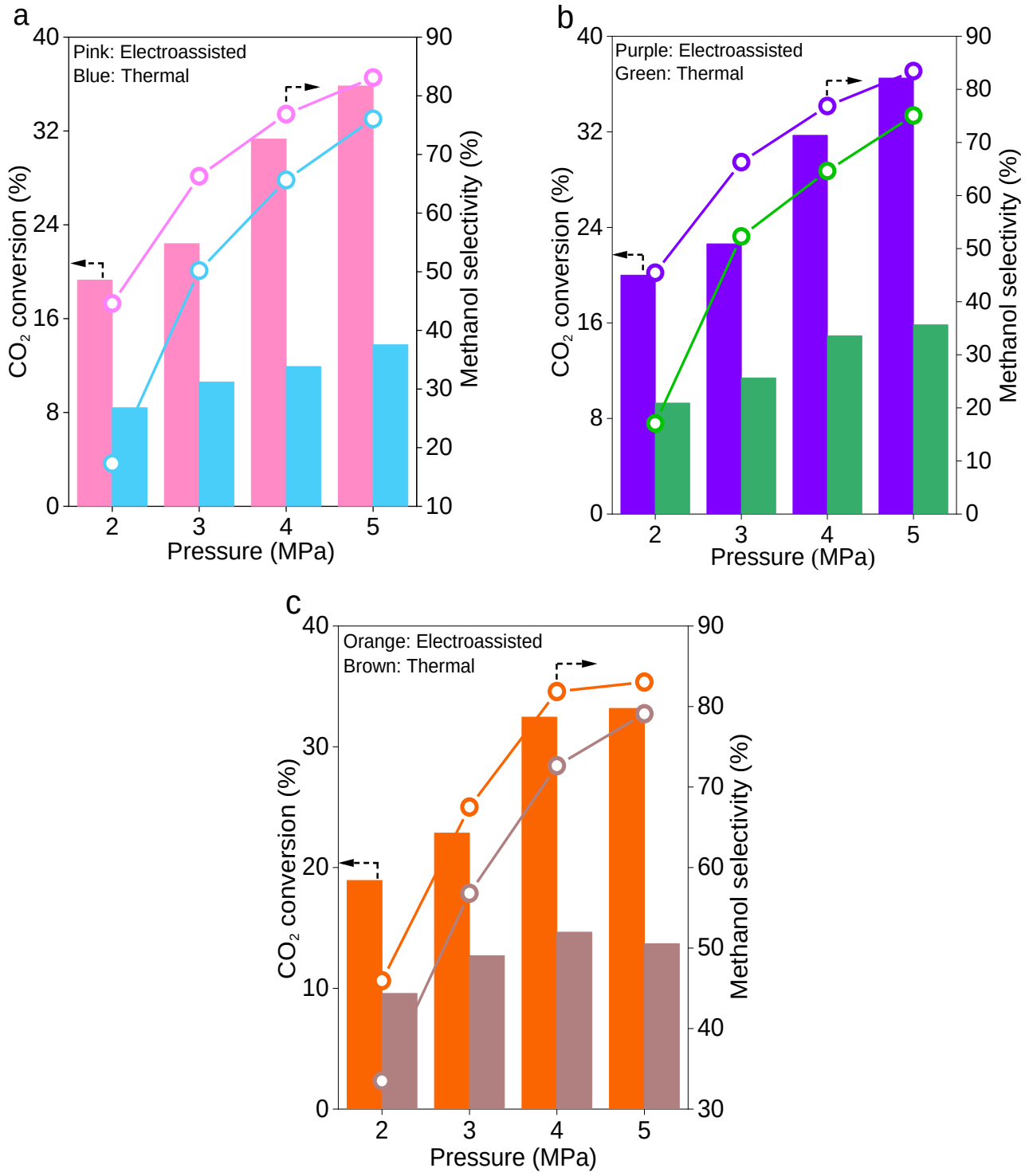

Supplementary Fig. 19 Effect of pressure on the electroassisted catalytic CO_2 selective hydrogenation to methanol on (a) 52%CZA, (b) 57%CZA and (c) 65%CZA at 240°C, 0.5 W, 3.0 MPa, 2000 $mL \cdot g_{Cat}^{-1} \cdot L^{-1}$ and H_2/CO_2 ratio = 3 compared those results obtained under thermal condition.

Supplementary Table 3 Catalytic performance of reported catalysts on CO_2 hydrogenation to methanol at comparable reaction conditions

Catalyst	H_2/CO_2 ratio	Space velocity ($mL \cdot g_{cat}^{-1} \cdot h^{-1}$)	P (MPa)	T (^oC)	Power (W)	Specific activity ($mmol \cdot g_{cat}^{-1} \cdot h^{-1}$)	Sel. (%)	Ref.
CZG-5Ga	2.8	N/A	4.5	240	-	N/A	49.0	1
$PdCu/ZrO_2$	3.0	3600	4.1	250	-	1.63	26.8	2
$PdCu/Al_2O_3$	3.0	3600	4.1	250	-	1.50	31.4	
$Pd/Cu/SiO_2$	3.0	3600	4.1	250	-	0.87	34.0	3
$Cu/ZrO_2/CNT$	3.0	3600	3.0	260	-	2.62	43.5	4
S-CuZnZr	3.0	3600	3.0	240	-	1.25	73.4	5
CuZnZr	3.0	3600	3.0	240	-	1.11	38.6	
CuZnAlZr	3.0	4600	5.0	230	-	5.52	62.1	6
Cu(ZnGa)	3.0	3000	3.0	250	-	0.31	37.8	7
	3.0	3000	3.0	260	-	0.45	38.1	
(CuZnGa)	3.0	3000	3.0	250	-	1.32	42.8	
	3.0	3000	3.0	260	-	1.46	36.5	
$Cu/ZnO/ZrO_2$	3.0	2400	3.0	240	-	1.98	41.0	8
CuZnAl	3.0	3600	3.0	240	-	3.73	63.6	9
	3.0	3600	3.0	240	-	3.04	62.6	
Cu/ZnOx@UiO-66	3.0	3600	3.0	240	-	0.69	53.9	10
	3.0	2400	3.0	240	-	0.08	49.2	
LDO	2.5	2000	4.0	230	-	1.35	39.5	11
CCZ	3.0	3600	3.0	260	-	2.88	50.0	12
Cu/TiO_2	3.0	3600	3.0	260	-	2.07	64.7	13
$PdCu/SiO_2$	3.0	3600	4.1	250	-	0.78	30.0	14
	3.0	3600	4.1	250	-	0.87	34.0	
PdCu/SBA-15	3.0	3600	4.1	250	-	0.58	23.0	
PdCu/MSU	3.0	3600	4.1	250	-	0.37	18.0	
$Cu-Zn/SiO_2$	3.0	3600	4.1	250	-	0.42	50.0	

$Cu\text{-}ZnO\text{-}Al_2O_3$	3.0	3600	4.1	250	-	1.92	27.0	
$CuO\text{-}ZnO/ZrO_2$	3.0	3600	3.0	240	-	3.84	56.2	15
La-Zr-Cu-ZnO	3.0	3600	5.0	250	-	2.74	52.5	16
Pd/Ga_2O_3	3.0	6000	5.0	250	-	5.74	51.6	17
$CuCeTiO_x$	3.0	2000	3.0	235	-	0.51	35.0	18
$Ga_{0.4}In_{1.6}O_3$	4.0	4500	3.0	320	-	1.35	28.0	19
$Pd/CNT+ZnZrO_x$	4.0	24000	5.0	240	-	5.21	81.8	20
Pd_1In_5/Al_2O_3	3.0	9000	3.0	260	-	1.58	82.2	21
$Cu_{0.25}In_{0.75}Zr_{0.5}O$	3.0	18000	2.5	250	-	2.40	79.7	22
$Cu\text{-}Zn/SiO_2$	3.0	60000	2.5	230	-	2.28	83.0	23
$Cu/Mo_2CT_x/SiO_2$	3.0	59600	2.5	230	-	1.90	52.0	24
$Co@Si_{0.95}$	3.0	6000	2.0	320	-	3.00	70.5	25
$Pd@8cGa_2O_3$	3.0	15000	4.5	250	-	5.90	70.4	26
CuZn@UiO-bpy	3.0	18000	4.0	250	-	0.0056	100	27
$Cu/BaTiO_{2.8}H_{0.2}$	3.0	6000	3.0	250	-	0.63	68.0	28
57%CZA	3.0	2000	3.0	240	0.5	5.46	64.3	**This work**
	3.0	2000	3.0	240	2.5	6.38	69.2	
	3.0	2000	4.0	240	0.5	5.94	76.9	
	3.0	2000	4.0	240	2.5	6.94	79.6	
	3.0	2000	5.0	240	0.5	6.53	83.5	
	3.0	2000	5.0	240	2.5	7.42	85.3	

Supplementary Table 4 Cu crystal size calculated by the most intensive Cu (111) peak using Debye-Scherrer formula

Catalyst sample	Cu crystal size (nm)
Fresh_Thermal treatment	11.2
Fresh_Electroassisted treatment	11.4
Spent_Thermal-200 h	15.0
Spent_Thermal-CO-150 h	12.9

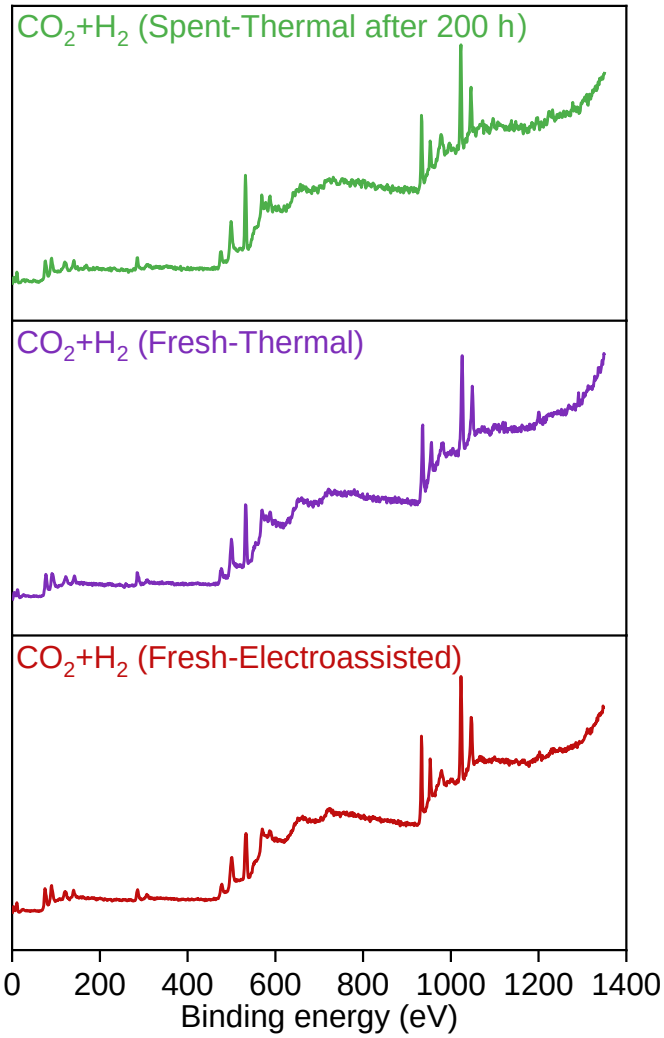

Supplementary Fig. 20 XPS survey spectra of spent 57%CZA catalyst sample collected after 200 h time-on-stream at the conditions of 240→280°C, 3 MPa, $H_2/CO_2/N_2$=72/24/4 mL·min^{-1} and 2000 mL·g_{Cat}^{-1}·h^{-1}, and those fresh sample after treatment under thermal and electroassisted condition.

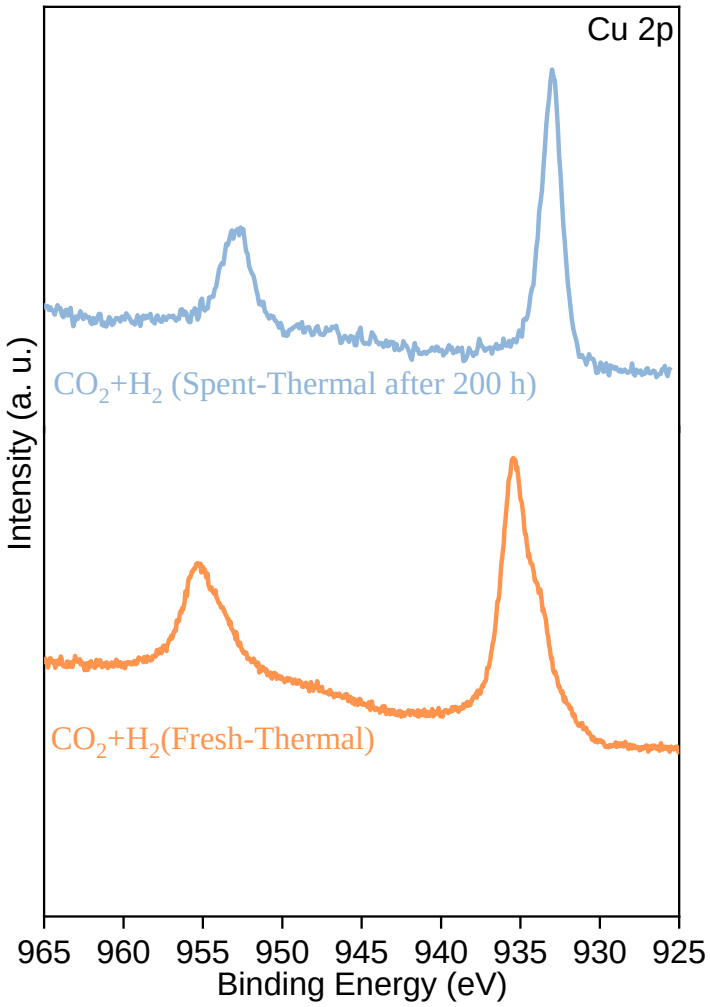

Supplementary Fig. 21 Cu 2p XPS fine spectra of spent 57%CZA catalyst sample collected after 200 h time-on-stream at the conditions of 240→280ºC, 3 MPa, $H_2/CO_2/N_2$=72/24/4 mL·min^{-1} and 2000 mL·g_{Cat}^{-1}·h^{-1}, compared with those fresh sample after treatment under thermal and electroassisted condition.

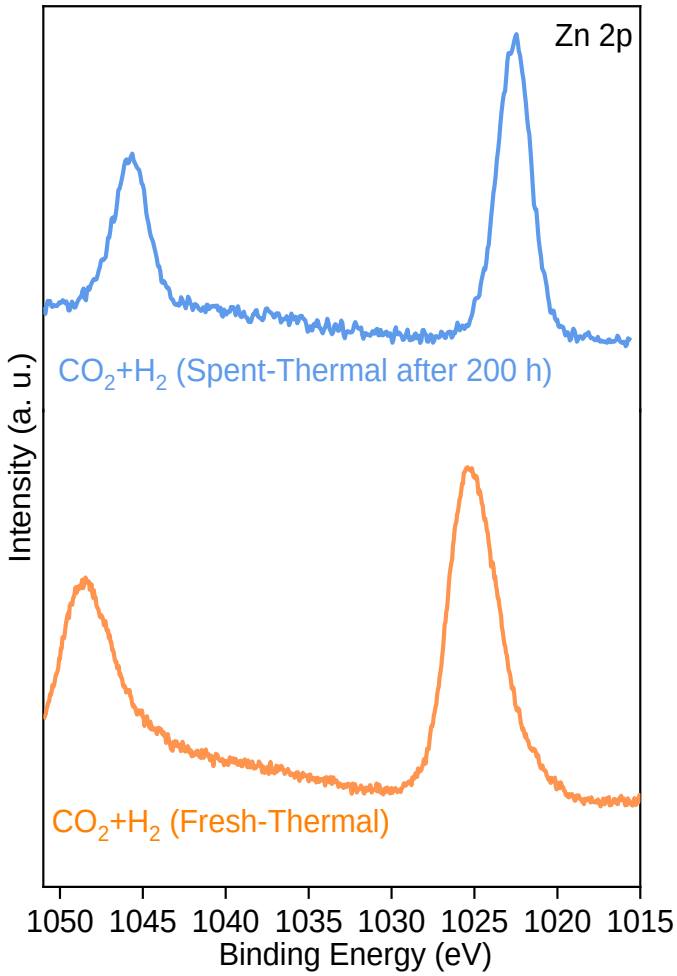

Supplementary Fig. 22 Zn 2p XPS fine spectra of spent 57%CZA catalyst sample collected after 200 h time-on-stream at the conditions of 240→280ºC, 3 MPa, $H_2/CO_2/N_2$=72/24/4 mL·min^{-1}, 2000 mL·g_{Cat}^{-1}·h^{-1} and 0.5 W (only for the electroassisted process) compared with those fresh sample after treatment under thermal and electroassisted condition without CO.

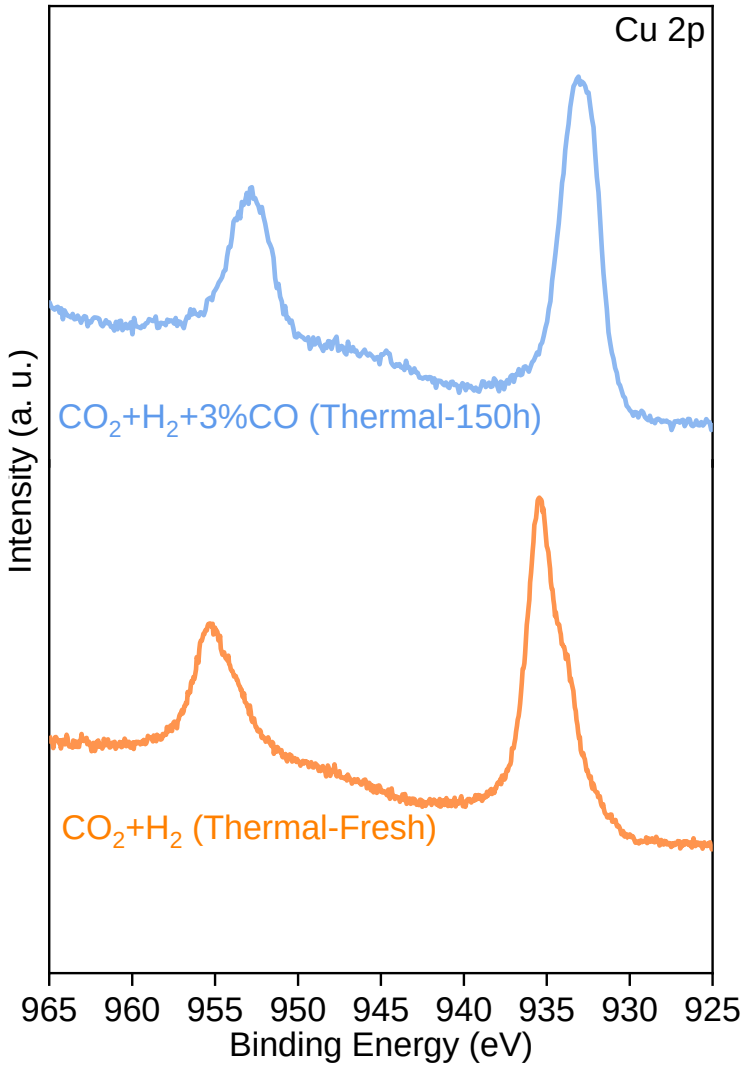

Supplementary Fig. 23 Cu 2p XPS fine spectra of spent 57%CZA catalyst sample collected after 150 h time-on-stream at the conditions of 240ºC, 3 MPa, $H_2/CO_2/CO/N_2$=72/21/3/4 mL·min^{-1}, 2000 mL·g_{Cat}^{-1}·h^{-1} and 0.5 W (only for the electroassisted process) compared with those fresh sample after treatment under thermal and electroassisted condition without CO.

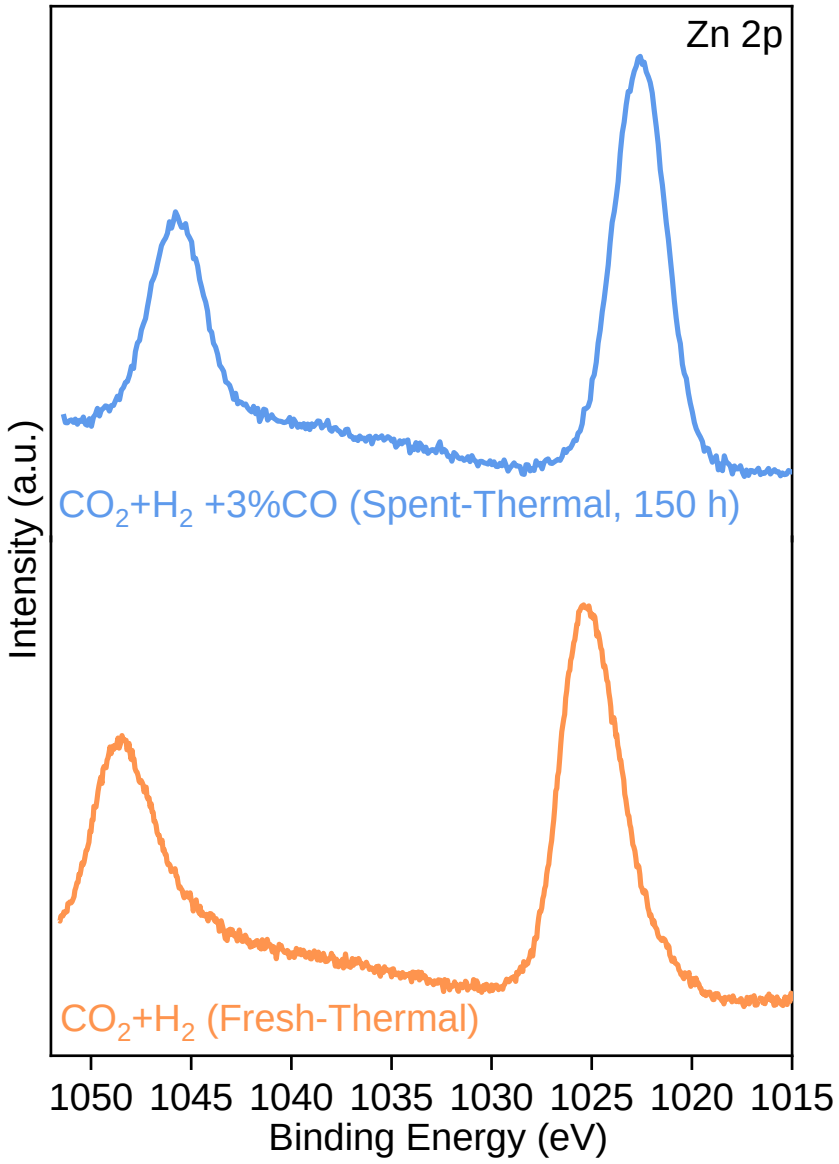

Supplementary Fig. 24 Zn 2p XPS fine spectra of spent 57%CZA catalyst sample collected after 150 h time-on-stream at the conditions of 240ºC, 3 MPa, $H_2/CO_2/CO/N_2$=72/21/3/4 mL·min^{-1}, 2000 mL·g_{Cat}^{-1}·h^{-1} and 0.5 W (only for the electroassisted process) compared with those fresh sample after treatment under thermal and electroassisted condition without CO.

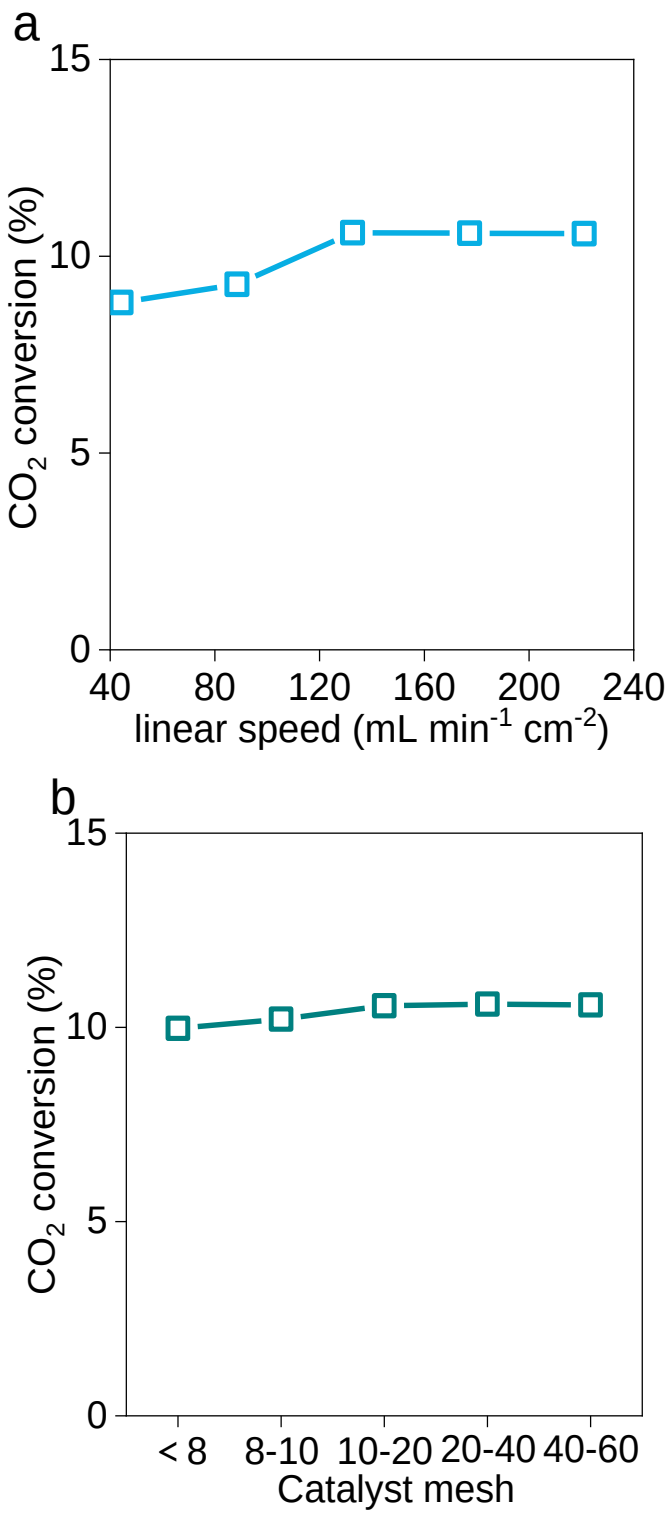

Supplementary Fig. 25 Experimental results of (a) external and (b) internal diffusion elimination under thermally catalytic condition.

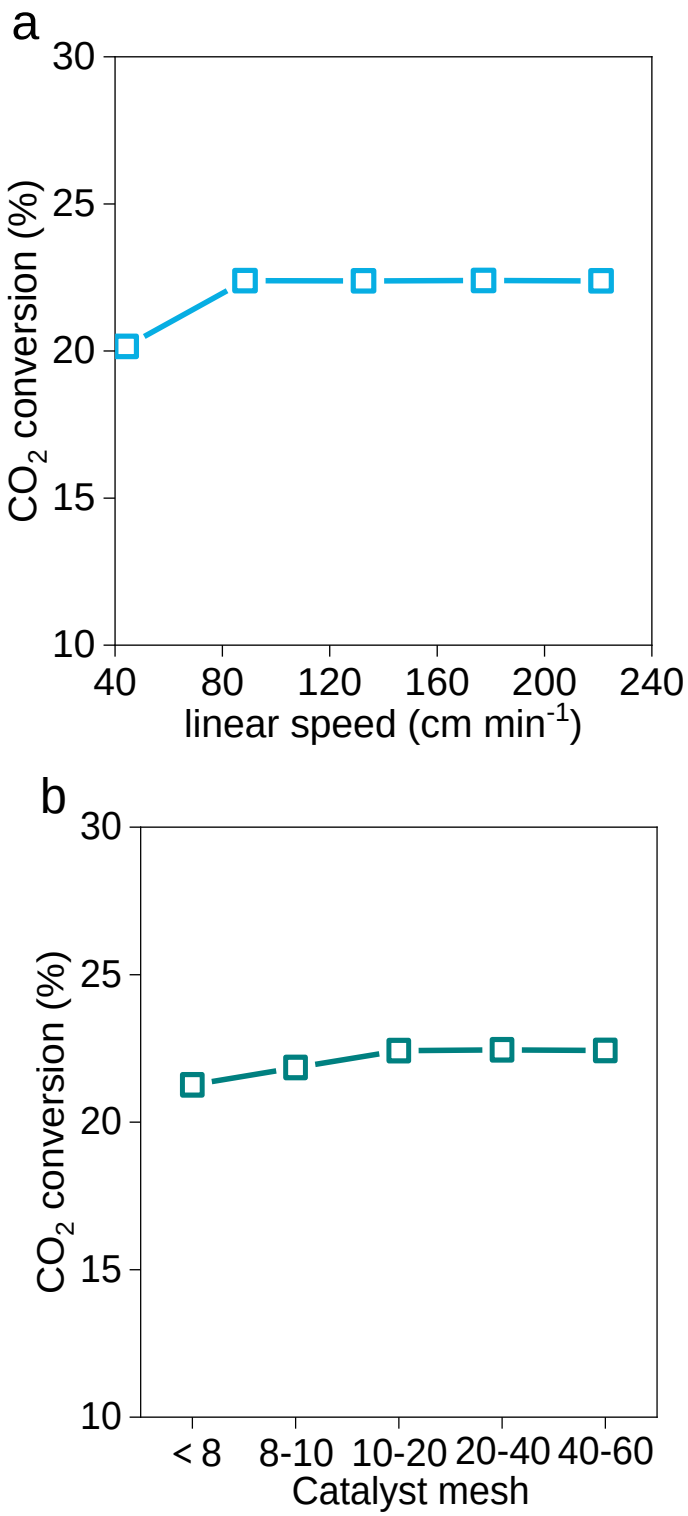

Supplementary Fig. 26 Experimental results of (a) external and (b) internal diffusion elimination under electroassisted catalytic condition.

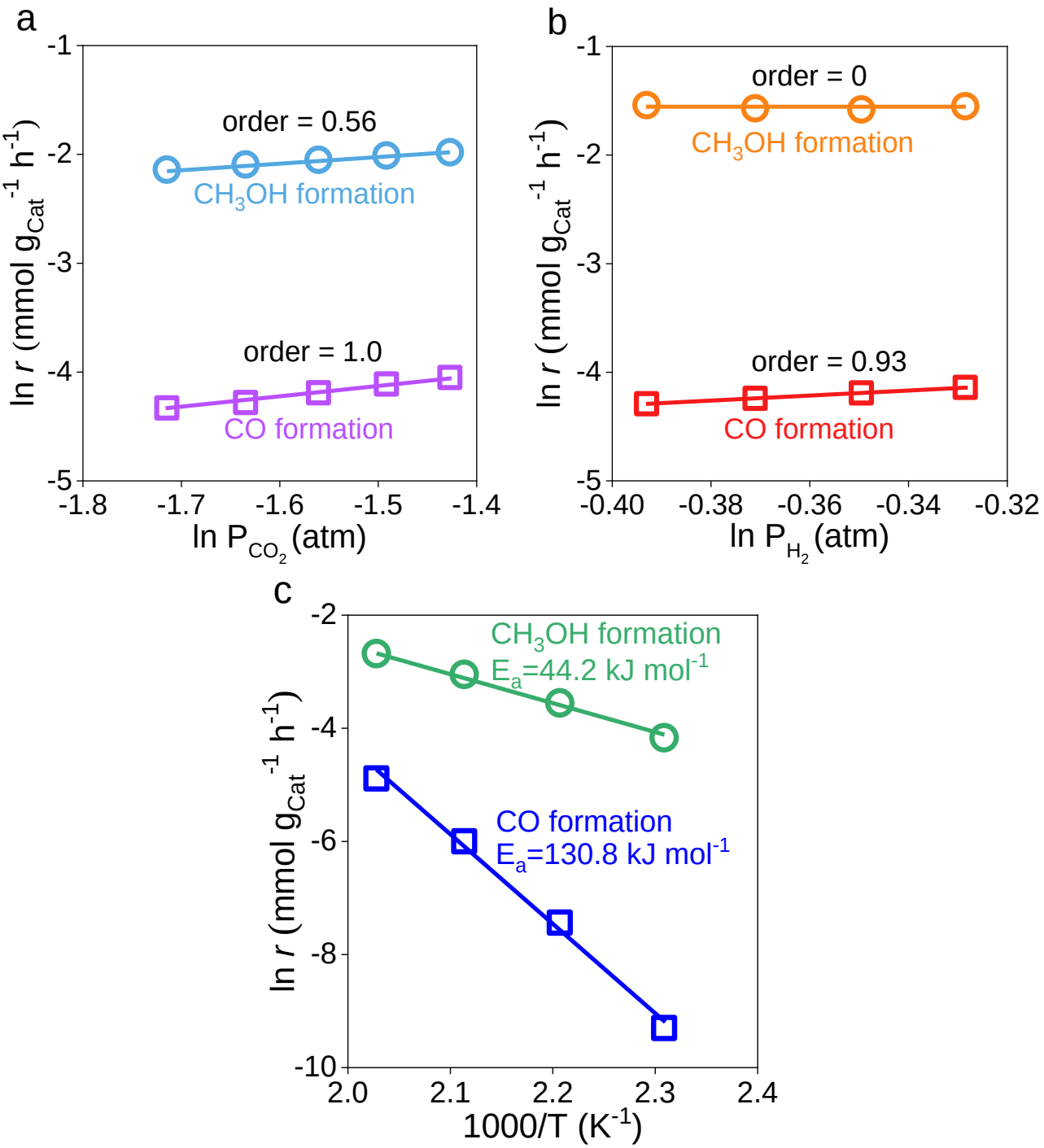

Supplementary Fig. 27 Kinetic studies on thermally catalytic CO_2 hydrogenation over 52%CZA (1 g) at the conditions of 160-220°C, 3 MPa, 0.5 W and 12000 $mL \cdot g_{Cat}^{-1} \cdot h^{-1}$. Dependency of methanol and CO formation on the concentration of (a) CO_2 and (b) H_2. (c) Arrhenius plots of CO_2 hydrogenation to methanol and CO under the H_2/CO_2 ratio of 3.

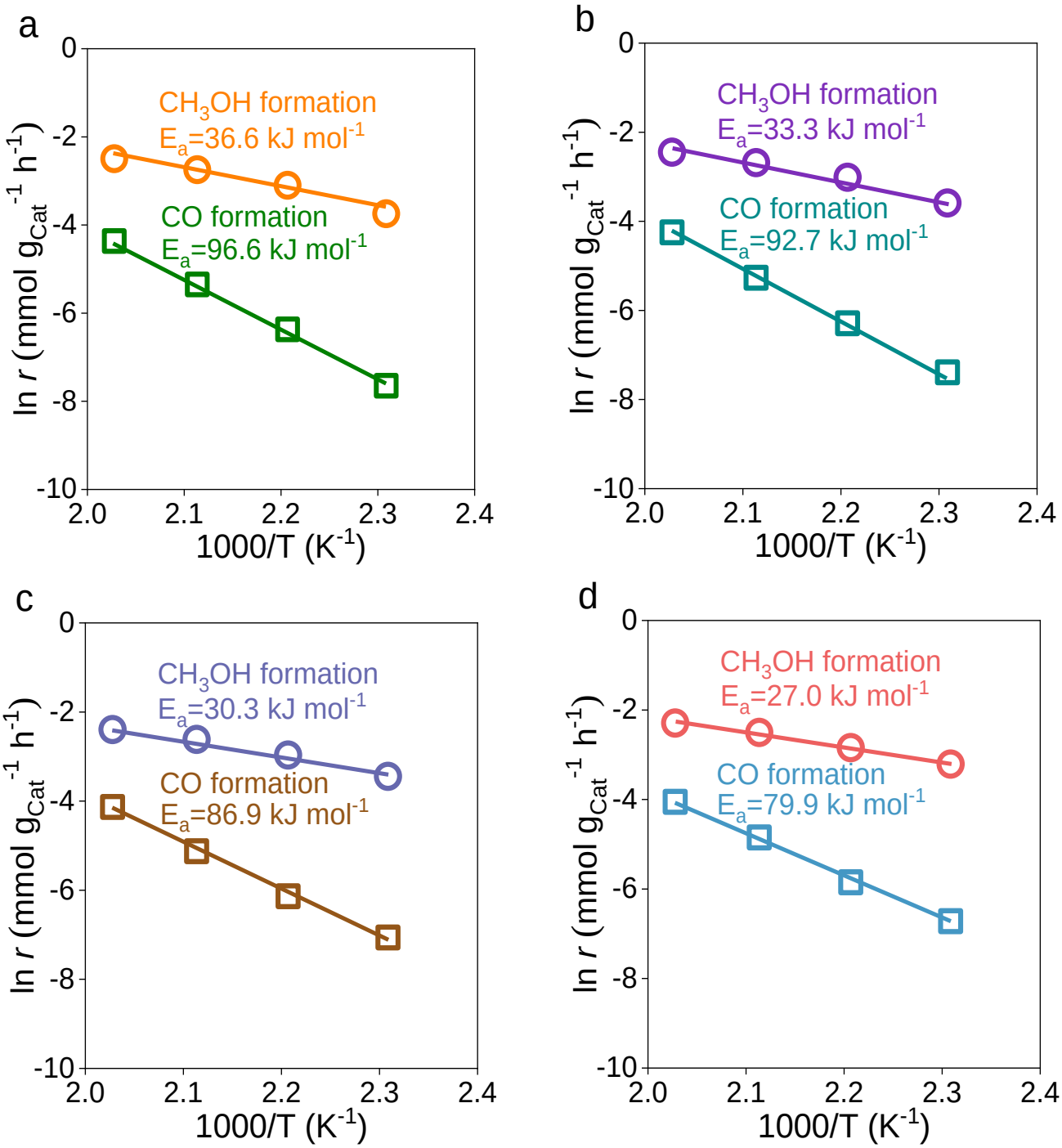

Supplementary Fig. 28 Arrhenius plots of electroassisted CO_2 hydrogenation under (a) 1.0 W, (b) 1.5 W, (c) 2.0 W and (d) 2.5 W at the conditions of 160-220°C, 3 MPa, H_2/CO_2 ratio of 3 and 12000 mL·g_{Cat}^{-1}·h^{-1}.

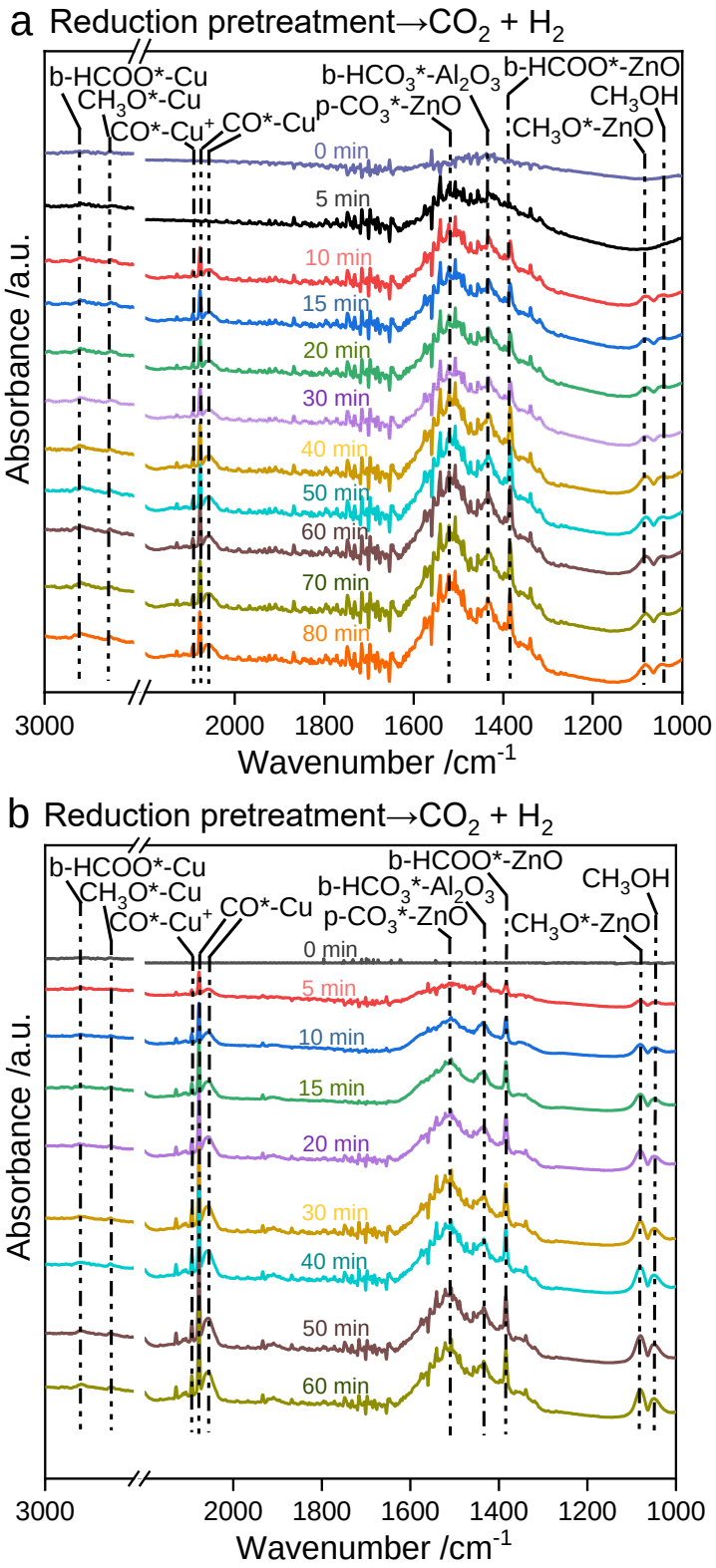

Supplementary Fig. 29 *In-situ* FT-IR spectra collected during (a) thermal and (b) electroassisted CO_2 hydrogenation on 57%CZA catalyst sample after reduction pretreatment using 10%H_2/N_2 at the conditions of 240°C, 0.1 MPa, CO_2/H_2=10/30 mL·min^{-1}, and 2.5 W (only for the electroassisted process).

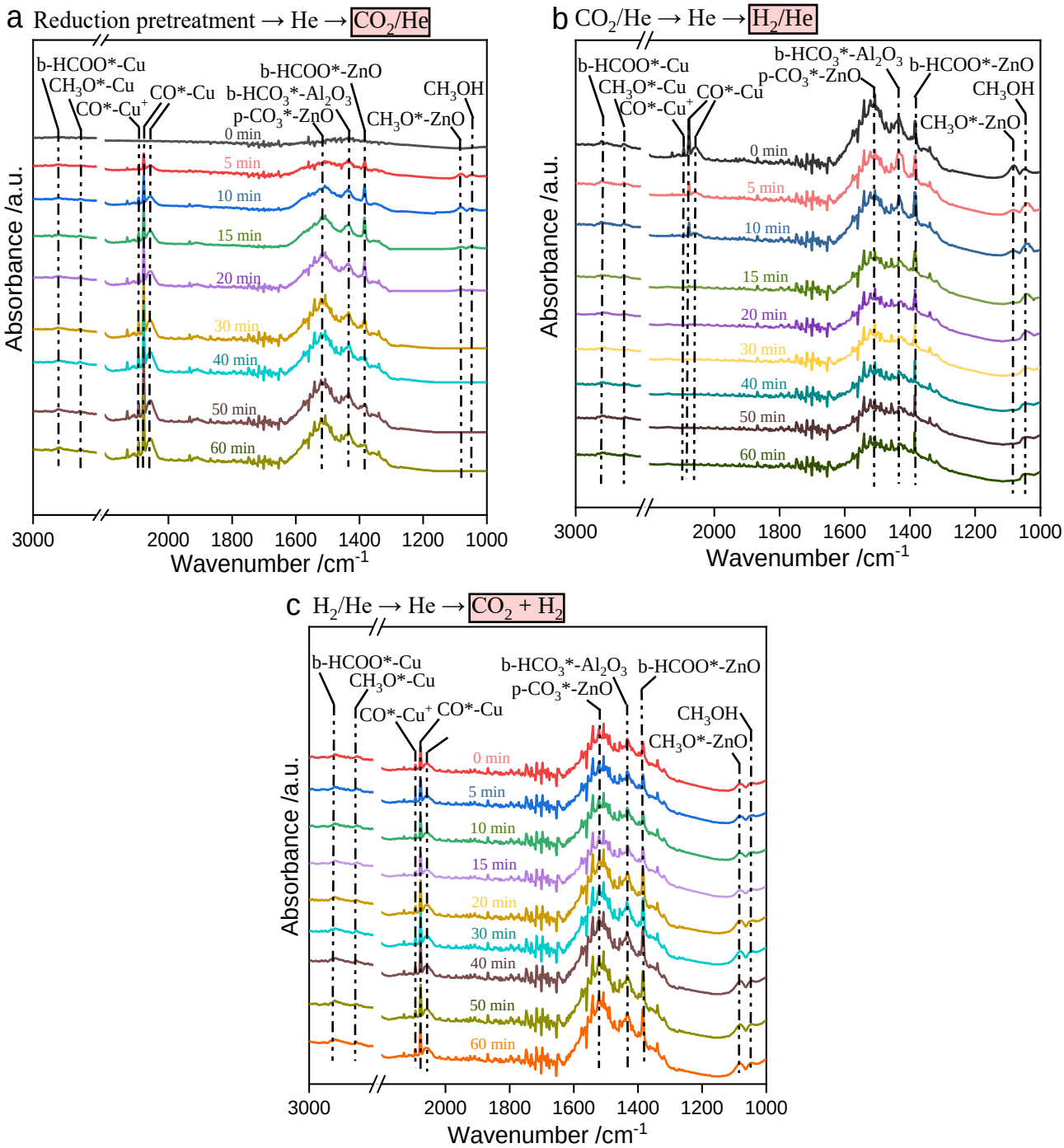

Supplementary Fig. 30 *In-situ* FT-IR spectra collected during thermal CO_2 hydrogenation over on 57%CZA catalyst sample at the stage of flowing (a) CO_2/He=10/30 mL·min^{-1}, (b) H_2/He=30/10 mL·min^{-1} and (c) CO_2/H_2=10/30 mL·min^{-1} at the conditions of 240°C, 0.1 MPa.

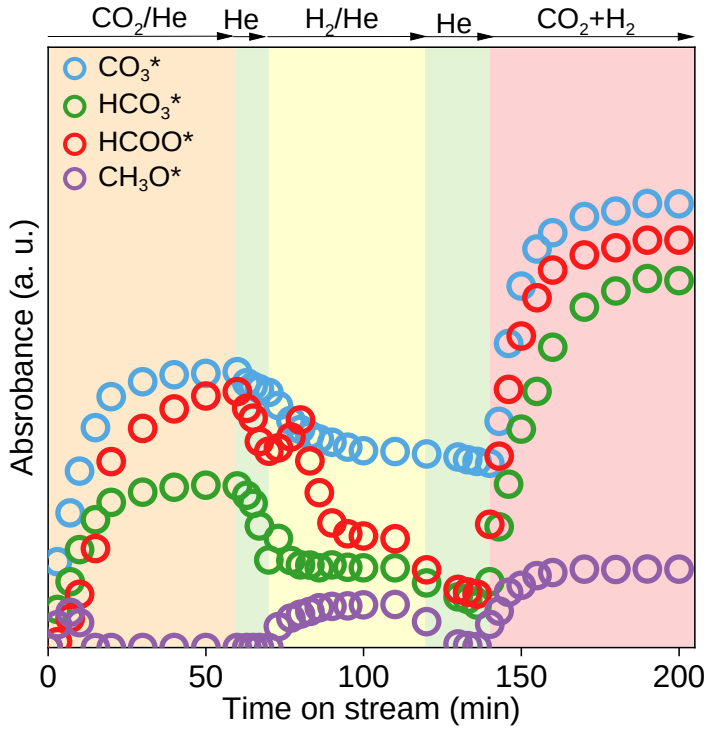

Supplementary Fig. 31 Evolution of reaction intermediates during the sequential gas flow of CO_2/He=10/30 mL·min^{-1}, 40 mL·min^{-1} He, H_2/He=30/10 mL·min^{-1}, 40 mL·min^{-1} He, and CO_2/H_2=10/30 mL·min^{-1} for thermal CO_2 hydrogenation to methanol at the conditions of 240°C and 0.1 MPa.

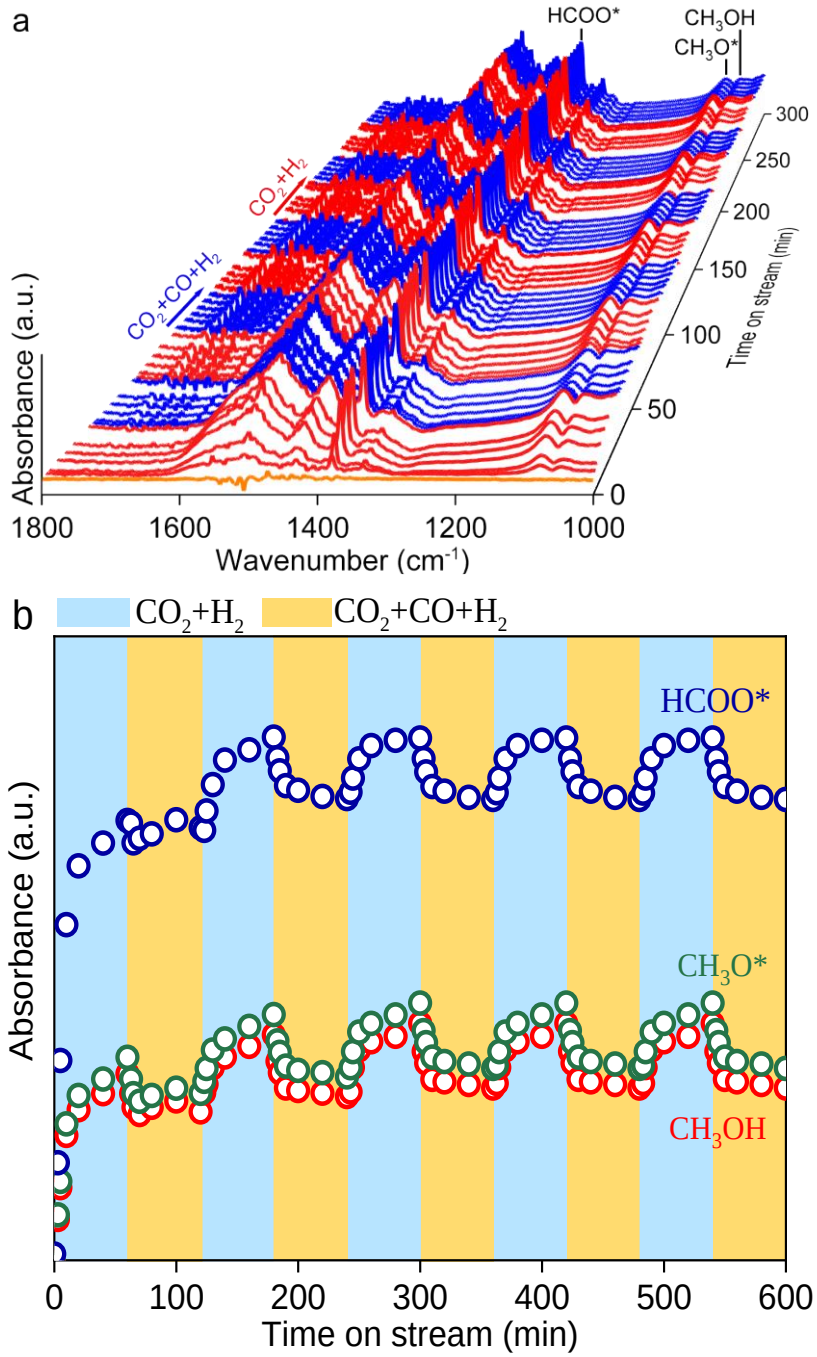

Supplementary Fig. 32 *In-situ* FT-IR spectroscopic experiment for the investigation on the effect of CO on thermal CO_2 hydrogenation to methanol at the conditions of 240°C, 0.1 MPa, CO_2/H_2=25/75 mL·min^{-1}, $CO_2/CO/H_2$=22/3/75 mL·min^{-1}.

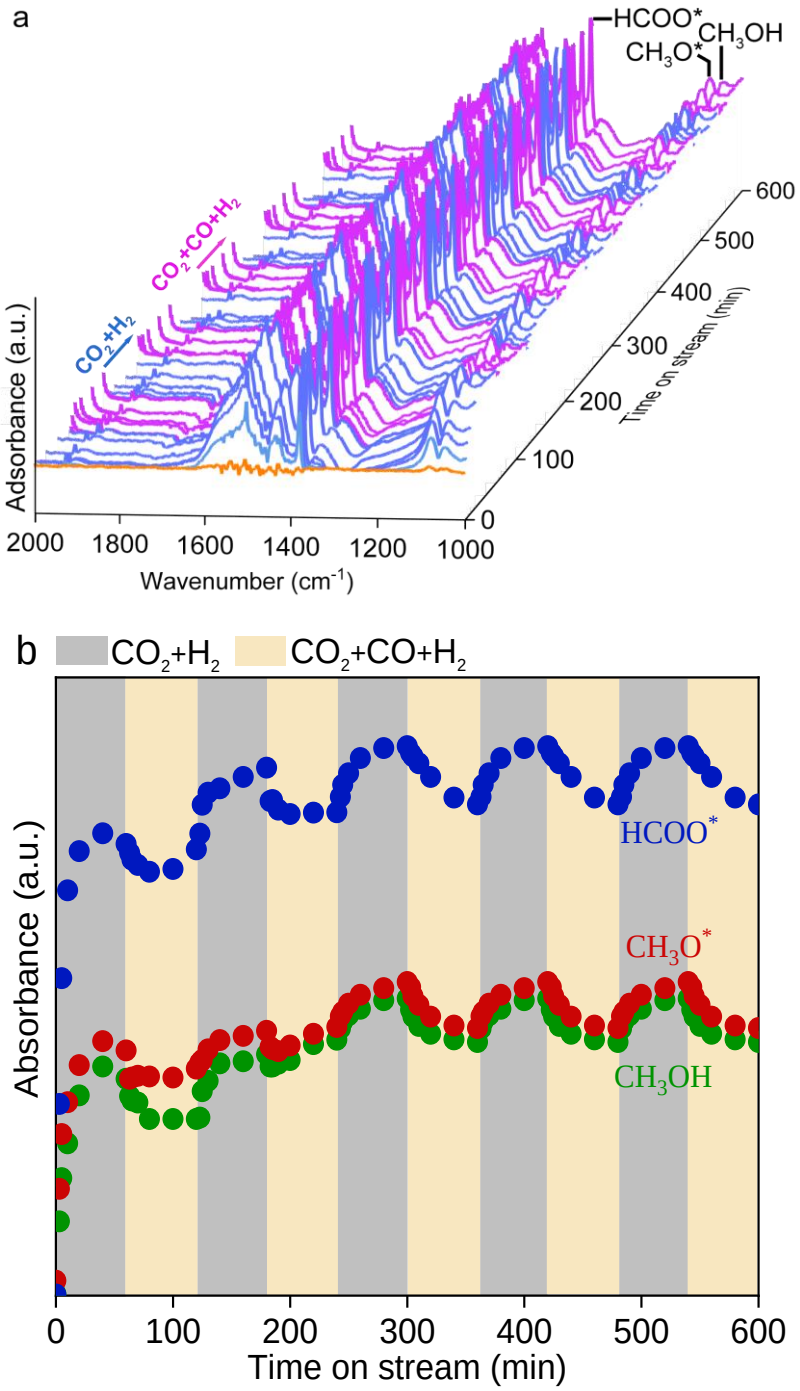

Supplementary Fig. 33 *In-situ* FT-IR spectroscopic experiment for the investigation on the effect of CO on electroassisted CO_2 hydrogenation to methanol at the conditions of 240°C, 0.1 MPa, CO_2/H_2=25/75 mL·min^{-1}, $CO_2/CO/H_2$=22/3/75 mL·min^{-1} and 0.5 W.

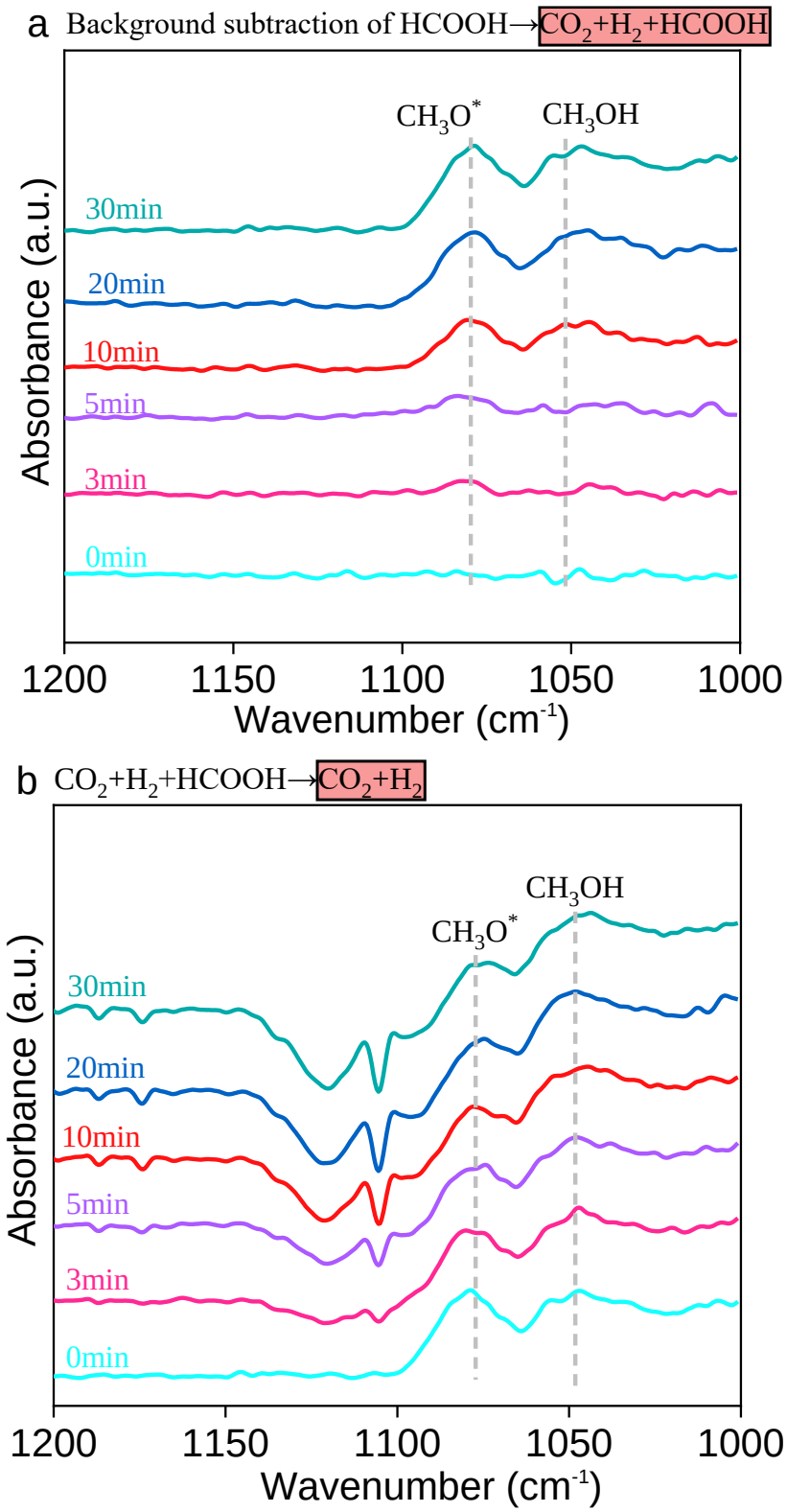

Supplementary Fig. 34 *In-situ* FT-IR spectroscopic experiment for the investigation on the effect of HCCOH on thermal CO_2 hydrogenation to methanol at the conditions of 240°C, 0.1 MPa and CO_2/H_2=25/75 mL·min^{-1} with HCCOH bubbled into IR cell.

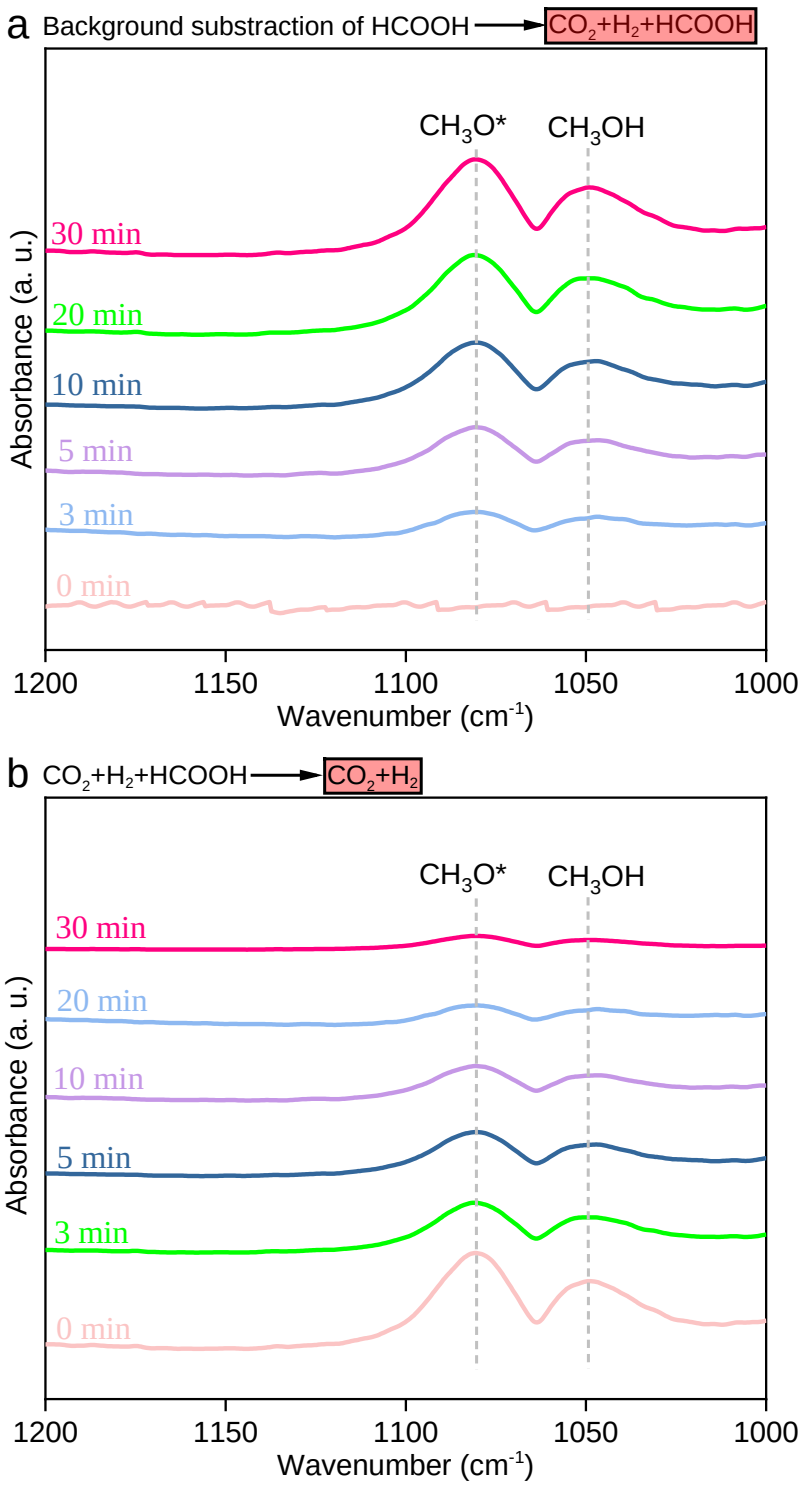

Supplementary Fig. 35 *In-situ* FT-IR spectroscopic experiment for the investigation on the effect of HCCOH on electroassisted CO_2 hydrogenation to methanol at the conditions of 240°C, 0.1 MPa, CO_2/H_2=25/75 mL·min^{-1} and 0.5 W with HCOOH bubbled into IR cell.

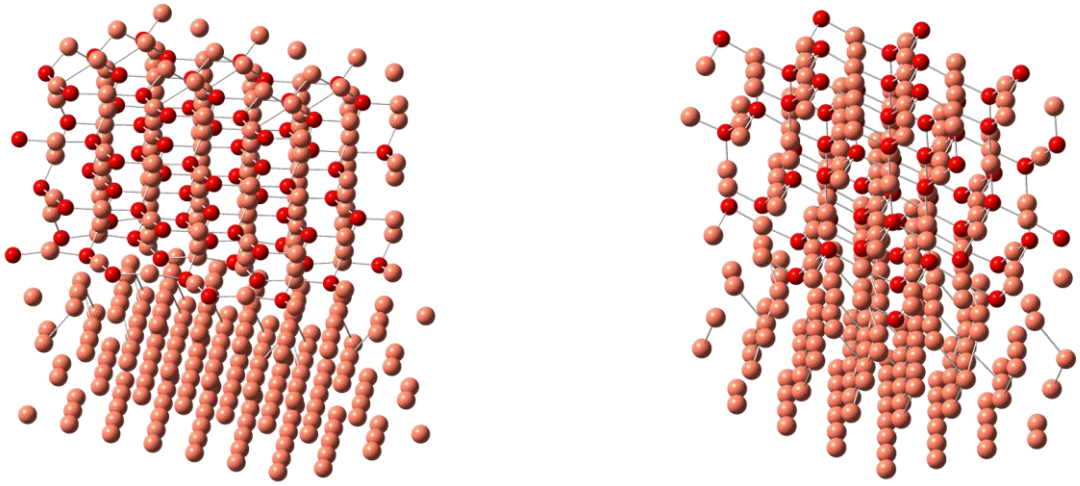

Cu(111)/Cu_2O(110) Cu(111)/Cu_2O(111)

Supplementary Fig. 36 Side view of proposed models for Cu(111)/Cu_2O(110) and Cu(111)/Cu_2O(111)

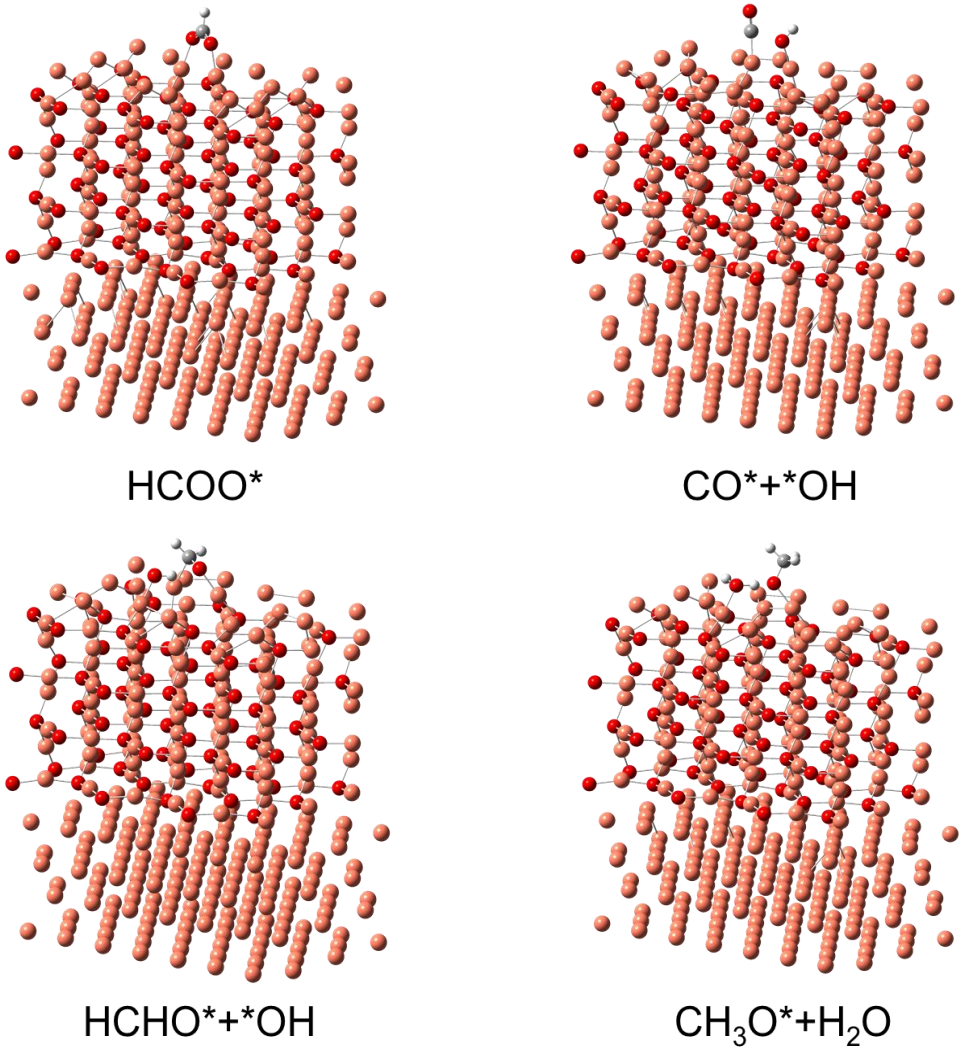

Supplementary Fig. 37 Configurations of different intermediate species absorbed on the model of Cu(111)/Cu_2O(110)

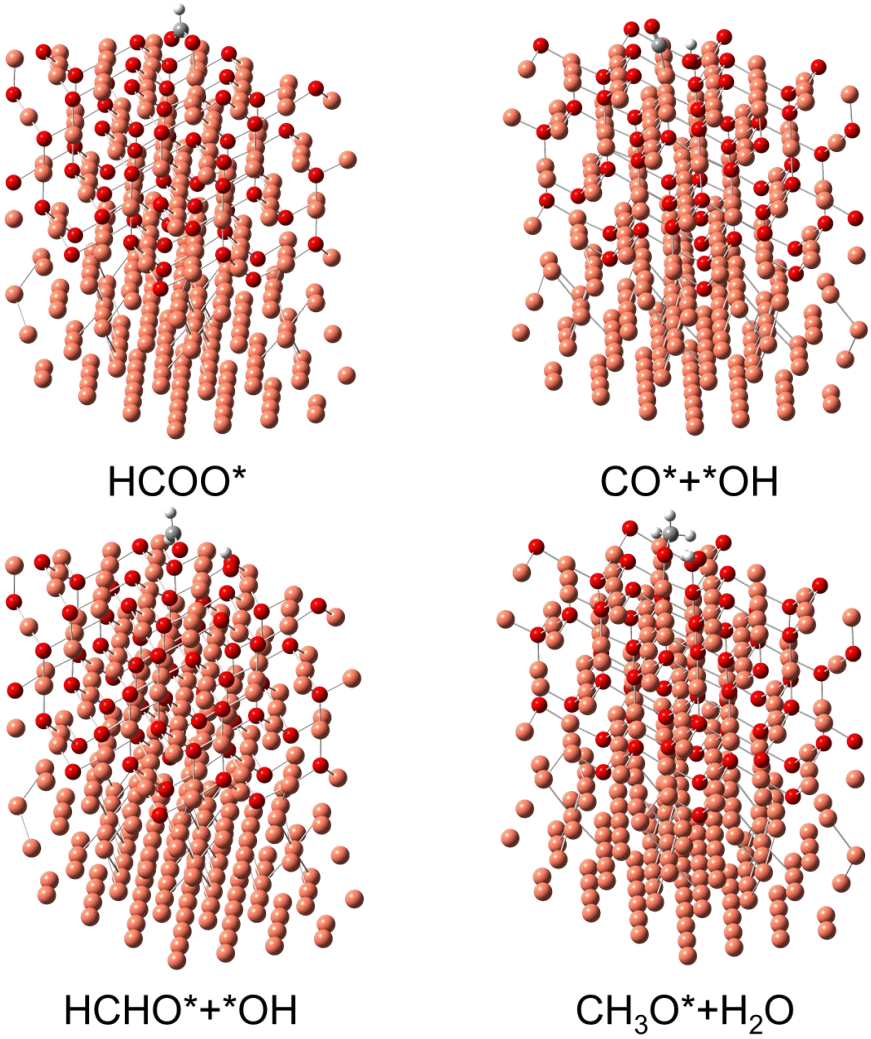

Supplementary Fig. 38 Configurations of different intermediate species absorbed on the model of $Cu(111)/Cu_2O(111)$

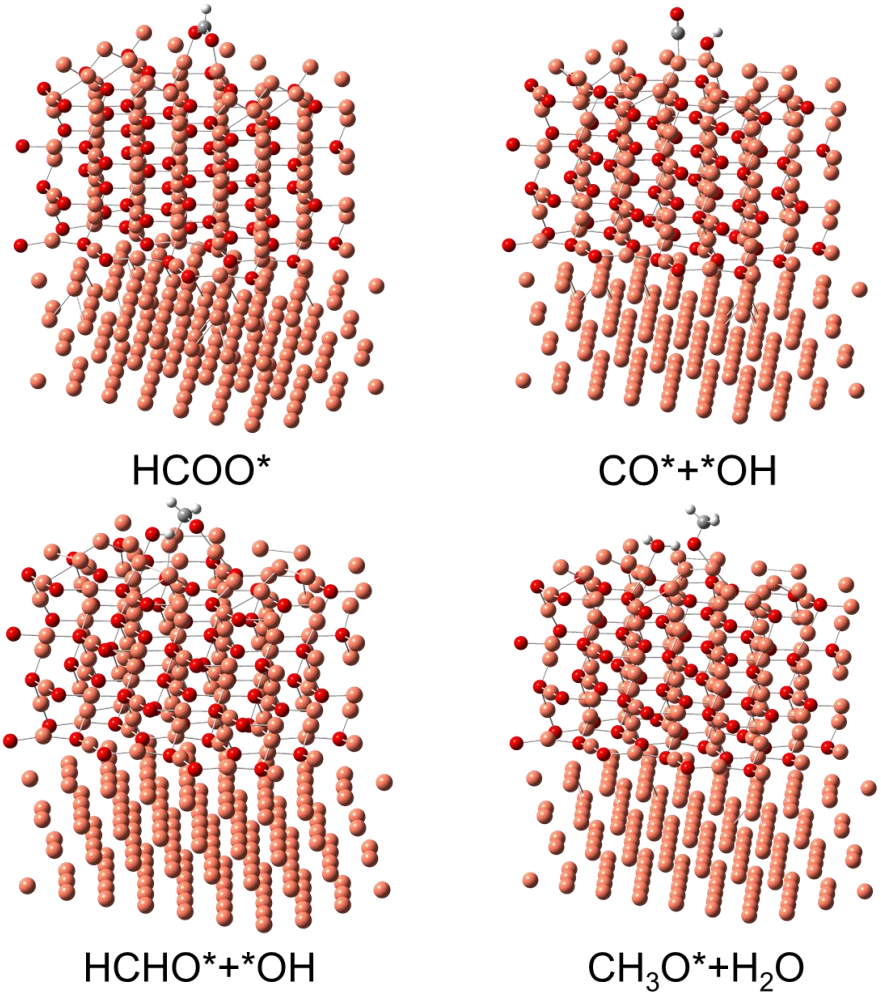

Supplementary Fig. 39 Configurations of different intermediate species absorbed on the model of $Cu(111)/Cu_2O(110)$ when 0.0001au electric power is introduced into the system

References

[1] M. J. Li, Z. Zeng, F. Liao, X. Hong, S. C. E. Tsang, Enhanced CO_2 hydrogenation to methanol over CuZn nanoalloy in Ga modified Cu/ZnO catalysts, *J*. *Catal*. **2016**, *343*, 157-167.

[2] F. W. Lin, X. Jiang, N. Boreriboon, Z. H. Wang, C. S. Song, K. F. Cen, Effects of supports on bimetallic Pd-Cu catalysts for CO_2 hydrogenation to methanol, *Appl*. *Catal*. *A*-Gen **2019**, *585*, 117210.

[3] X. Jiang, N. Koizumi, X. W. Guo, C. S. Song, Bimetallic Pd-Cu catalysts for selective CO_2 hydrogenation to methanol, *Appl*. *Catal*. *B-Environ*. **2015**, *170*, 173-185.

[4] G. N. Wang, L. M. Chen, Y. H. Sun, J. L. Wu, M. L. Fu, D. Q. Ye, Carbon dioxide hydrogenation to methanol over Cu/ZrO_2/CNTs: Effect of carbon surface chemistry, *RSC Adv.* **2015,** *5*, 45320-45330.

[5] L. Li, D. S. Mao, J. Yu, X. M. Guo, Highly selective hydrogenation of CO_2 to methanol over CuO-ZnO-ZrO_2 catalysts prepared by a surfactant-assisted co-precipitation method, *J*. *Power Sources* **2015**, *279*, 394-404.

[6] X. S. Dong, F. Li, N. Zhao, Y. S. Tan, J. W. Wang, F. K. Xiao, CO_2 hydrogenation to methanol over Cu/Zn/Al/Zr catalysts prepared by liquid reduction, *Chinese J*. *Catal*. **2017**, *38*, 717-725.

[7] W. J. Cai, P. R. de la Piscina, J. Toyir, N. Homs, CO_2 hydrogenation to methanol over CuZnGa catalysts prepared using microwave-assisted methods, *Catal. Today* **2015**, *242*, 193-199.

[8] G. Wang, D. S. Mao, X. M. Guo, J. Yu, Methanol synthesis from CO_2 hydrogenation over CuO-ZnO-ZrO_2-M_xO_y catalysts (M=Cr, Mo and W), *Int*. *J*. *Hydrogen Energ*. **2019**, *44*, 4197-4207.

[9] H. Lei, Z. Y. Hou, J. W. Xie, Hydrogenation of CO_2 to CH_3OH over CuO/ZnO/Al_2O_3 catalysts prepared via a solvent-free routine, *Fuel* **2016**, *164*, 191-198.

[10] J. Yu, G. Q. Chen, Q. S. Guo, X. M. Guo, P. Da Costa, D. S. Mao, Ultrasmall bimetallic Cu/ZnO_x nanoparticles encapsulated in UiO-66 by deposition-precipitation method for CO_2 hydrogenation to methanol, *Fuel* **2022**, 324, 124694.

[11] J. Tian, W. X. Qian, H. T. Zhang, H. F. Ma, W. Y. Ying, Synthesis of methanol over highly dispersed Cu-Fe based catalysts derived from layered double hydroxides, *RSC Adv*. **2023**, *13*, 13902-13910.

[12] G. N. Wang, L. M. Chen, Y. Y. Guo, M. L. Fu, J. L. Wu, B. C. Huang, D. Q. Ye, Effect of chromium doping on the catalytic behavior of $Cu/ZrO_2/CNTs\text{-}NH_2$ for the synthesis of methanol from carbon dioxide hydrogenation, *Acta Phys-Chim. Sin.* **2014**, *30*, 923-931.

[13] Y. F. Bao, C. L. Huang, L. M. Chen, Y. D. Zhang, L. Liang, J. J. Wen, M. L. Fu, J. L. Wu, D. Q. Ye, Highly efficient Cu/anatase TiO_2 {001}-nanosheets catalysts for methanol synthesis from CO_2, *J*. *Energ*. *Chem*. **2018**, 27, 381-388.

[14] X. Jiang, N. Koizumi, X. W. Guo, C. S. Song, Bimetallic Pd-Cu catalysts for selective CO_2 hydrogenation to methanol, *Appl*. *Catal*. *B-Environ*. **2015**, 170-171, 173-185.

[15] X. M. Guo, D. S. Mao, S. Wang, G. S. Wu, G. Z. Lu, Combustion synthesis of CuO-ZnO-ZrO_2 catalysts for the hydrogenation of carbon dioxide to methanol, *Catal*. *Commun*. **2009**, *10*, 1661-1664.

[16] H. J. Zhan, F. Li, P. Gao, N. Zhao, F. K. Xiao, W. Wei, L. S. Zhong, Y. H. Sun, Methanol synthesis from CO_2 hydrogenation over La-M-Cu-Zn-O (M = Y, Ce, Mg, Zr) catalysts derived from perovskite-type precursors, *J. Power Sources* **2014**, *251*, 113-121.

[17] X. W. Zhou, J. Qu, F. Xu, J. P. Hu, J. S. Foord, Z. Y. Zeng, X. L. Hong, S. C. E. Tsang, Shape selective plate-form Ga_2O_3 with strong metal-support interaction to overlying Pd for hydrogenation of CO_2 to CH_3OH, *Chem*. *Commun*. **2013**, *49*, 1747-1749.

[18] K. Chang, T. F. Wang, J. G. G. Chen, Hydrogenation of CO_2 to methanol over $CuCeTiO_x$ catalysts, *Appl*. *Catal*. *B-Environ*. **2017**, *206*, 704-711.

[19] N. Akkharaphatthawon, N. Chanlek, C. K. Cheng, M. Chareonpanich, J. Limtrakul, T. Witoon, *Appl*. *Surf*. *Sci*. **2019**, *489*, 278-286.

[20] K. Lee, P. C. D. Mendes, H. Jeon, Y. Z. Song, M. P. Dickieson, U. Anjum, L. W. Chen, T. C. Yang, C. M. Yang, M. Choi, S. M. Kozlov, N. Yan, *Nature Commun*. **2023**, *14*, 819.

[21] A. M. Alamer, M. Y. Ouyang, F. H. Alshafei, M. A. Nadeem, Y. Alsalik, J. T. Miller, M. Flytzani-Stephanopoulos, E. C. H. Sykes, V. Manousiouthakis, N. M. Eagan, *ACS. Catal*. **2023**, *13*, 9987-9996.

[22] L. B. Yao, X. C. Shen, Y. B. Pan, Z. M. Peng, *J*. *Catal*. **2019**, *372*, 74-85.

[23] H. Zhou, S. R. Docherty, N. Phongprueksathat, Z. X. Chen, A. V. Bukhtiyarov, I. P. Prosvirin, O. V. Safonova, A. Urakawa, C. Copéret, C. R. Müller, A. Fedorov, *JACS Au*, **2023**, *3*, 2536-2549.

[24] H. Zhou, Z. X. Chen, A. V. López, E. D. López, E. Lam, A. Tsoukalou, E. Willinger, D. A. Kuznetsov, D. Mance, A. Kierzkowska, F. Donat, P. M. Abdala, A. Comas-Vives, C. Copéret, A. Fedorov, C. R. Müller, *Nature Catal*. **2021**, *4*, 860-871.

[25] L. X. Wang, E. Guan, Y. Q. Wang, L. Wang, Z. M. Gong, Y. Cui, X. J. Meng, B. C. Gates, F. S. Xiao, *Nature Commun*. **2020**, *11*, 1033.

[26] X. Y. Liu, Q. Q. Gu, Y. F. Zhang, X. Y. Xu, H. W. Wang, Z. H. Sun, L. N. Cao, Q. M. Sun, L. L. Xu, L. L. Wang, S. Li, S. Q. Wei, B. Yang, J. L. Lu, *J*. *Am*. *Chem*. *Soc*. **2023**, *145*, 6702-6709.

[27] B. An, J. Z. Zhang, K. Cheng, P. F. Ji, C. Wang, W. B. Lin, *J*. *Am*. *Chem*. *Soc*. **2017**, *139*, 3834-3840.

[28] Y. He, Y. Y. Li, M. Lei, F. Polo-Garzon, J. Perez-Aguilar, S. R. Bare, E. Formo, H. Kim, L. Daemen, Y. Q. Cheng, K. L. Hong, M. F. Chi, D. E. Jiang, Z. L. Wu, *Angew*. *Chem*. *Int*. *Ed*. **2023**, Doi: 10.1002/anie.202313389.